Case study of developing African easterly wave during NAMMA: An energetic point of view

Joël Arnault, Frank Roux

Case Study of a Developing African Easterly Wave during NAMMA: An Energetic Point of View

JOËL ARNAULT AND FRANK ROUX

Université de Toulouse, UPS, Laboratoire d'Aérologie, and CNRS, Toulouse, France

(Manuscript received 13 November 2008, in final form 29 April 2009)

ABSTRACT

The West African perturbation that subsequently evolved into Hurricane Helene (2006) during NASA's African Monsoon Multidisciplinary Analysis (NAMMA), 15 August–14 September 2006, and AMMA's third special observing period (SOP-3), 15–29 September 2006, has been simulated with the nonhydrostatic Méso-NH model using parameterized convection. The simulated disturbance evolved over West Africa and the adjacent eastern tropical Atlantic through interactions between different processes at the convective scale, mesoscale, and synoptic scale. The aim of this paper is to quantify the energetics of the simulated disturbance. A set of energy equations is first developed in the hydrostatic case to solve the limitations of Lorenz's analysis when applied to a finite domain. It is shown that this approach is also valid in the compressible and in the anelastic case in order to apply it to the Méso-NH results. Application to the simulated pre-Helene disturbance allows one to determine the most important terms in these equations. These simplifications are taken into account to derive an energy cycle including barotropic and baroclinic conversions of eddy kinetic energy. The development of the simulated system was found to result from barotropic–baroclinic growth over West Africa and barotropic growth over the tropical eastern Atlantic. It is suggested that most of these energy conversions were the result of an adjustment of the wind field in response to the pressure decrease, presumably caused by convective activity.

1. Introduction

This work has two objectives: 1) to propose an energy budget adapted from Lorenz's (1955, hereafter L55) analysis in order to precisely quantify the growth of an African easterly wave (AEW) in a limited domain and 2) to apply this energy budget to the AEW that spawned Hurricane Helene (2006).

AEWs are wavelike disturbances observed in West Africa during the summer months. They have wavelengths of 3000–5000 km and periods of 3–5 days. Their amplitude is maximum at the level of the African easterly jet (AEJ) near 3000-m altitude (e.g., Erickson 1963; Burpee 1972). Norquist et al. (1977), following the energetic analysis in L55, showed that the growth of AEWs over West Africa is likely to be the consequence of a both barotropic and baroclinic instability of the AEJ. AEWs usually reach their maximal amplitude near the Guinean coast and start to decrease as they reach the tropical Atlantic Ocean, where baroclinic growth is reduced (e.g., Norquist et al. 1977; Thompson et al. 1979).

Several decades of observations have confirmed that a large proportion of Atlantic hurricanes evolve from AEWs (e.g., Avila and Clark 1989). However, few AEWs have a cyclogenetic evolution and the physical processes leading to such developments are not yet fully understood, although several hypotheses have been made. Landsea and Gray (1992) found a positive correlation between the Atlantic cyclonic activity and West Sahel rainfall variability during the summer months. This suggests that developing cases are the consequence of an interaction between AEWs and mesoscale convective systems (MCSs) that occur over West Africa during the monsoon period (we refer to the work of Laing et al. 2008 for an up-to-date description of West African MCSs during the monsoon season). Using statistics of AEWs in a 20-yr European Centre for Medium-Range Weather Forecasts (ECMWF) reanalysis dataset, Thorncroft and Hodges (2001) proposed that the cyclogenetic evolution of AEWs depends on their low-level amplitude when they leave the West African coast. Berry and Thorncroft

Corresponding author address: Joël Arnault, Laboratoire d'Aérologie, Observatoire Midi-Pyrénées, 14 avenue Edouard Belin, F-31400 Toulouse, France.
E-mail: joel.arnault@yahoo.fr

DOI: 10.1175/2009JAS3009.1

(2005) studied the AEW associated with the pre-Alberto (2000) disturbance over West Africa. They found that the cyclonic vorticity structure of this AEW merged with cyclonic vortices of convective origin over the Guinea Highlands, thus resulting in its intensification. They finally hypothesized that this interaction process between the AEW and MCSs led to the cyclogenesis of Alberto (2000), one day after the disturbance left the West African coast.

The interaction between AEWs and convection has also been investigated quantitatively with the L55 energetic analysis in several idealized case studies (e.g., Thorncroft 1995) and realistic simulations (e.g., Hsieh and Cook 2007). These authors found that the latent heat released by convection increases the baroclinic growth of AEWs, but they did not separate the developing cases from the nondeveloping ones. Using composite statistics on a 60-yr National Centers for Environmental Prediction (NCEP) reanalysis dataset, Aviles (2004) applied the L55 energetic analysis to differentiate developing AEWs from nondeveloping ones. Surprisingly, she found that ''the sources of eddy kinetic energy of developing AEWs are not as clearly barotropic and baroclinic as for nondeveloping ones'' (136–137). Indeed, the cyclogenetic evolution of AEWs does not depend as much on their energetic growth over West Africa as on their more or less favorable internal structure when they leave the West African coast (''anticyclonic flow in the upper levels and surrounding the positive vorticity center, deep rising motion, weak and small cold core, a moist environment;'' Aviles 2004, p. 140) and, to lesser extent, on a favorable environment in the Atlantic basin (e.g., Gray 1968).

Based on 15-yr ECMWF reanalyses, Kiladis et al. (2006) evaluated the adiabatic forcing of vertical motion with the divergence of **Q** vectors (Hoskins et al. 1978). They found ''strong correspondence between the dynamically forced vertical motion at 850 hPa and deep convection for the day −2 through day +1 stages of the AEW evolution along 10°N'' (2226–2227). In other words, vertical motions associated with AEWs in this region are mostly forced adiabatically, resulting in a simple relationship between convection and dynamics (convection occurs preferentially near the wave's trough; see, e.g., Payne and McGarry 1977). However, the divergence of **Q** vectors ''does a poor job in accounting for the more complicated vertical motion field for the 15°N, 17.5°W base point. This is in line with the likely important role of diabatic processes in the energetics of African easterly waves over some regions'' (Kiladis et al. 2006, p. 2227). Kiladis et al. (2006) concluded that the relationship between AEWs and convection could be precisely analyzed with vorticity and energy budgets.

Here, we study the energetics of the West African disturbance that spawned Hurricane Helene about 1000 km east of Cape Verde Islands on 16 September 2006, during NASA's African Monsoon Multidisciplinary Analysis (NAMMA) and AMMA's third special observing period (SOP-3). Our goal is to quantify the respective contributions of large-scale and internal processes involved in this developing case study. This case study has been numerically simulated with the French nonhydrostatic, anelastic model Méso-NH (Lafore et al. 1998), whose main characteristics are given in section 2. The results of this simulation are analyzed in section 3 and compared to *Meteosat-9* images in the water vapor channel at 7.3 μm. In section 4, we show the limits of L55's analysis when applied to the energetics of a disturbance in a finite domain, and we propose an alternate formulation for hydrostatic, compressible, and anelastic frameworks in a limited domain. In section 5, a scale analysis applied to the simulated pre-Helene disturbance allows us to separate the most important terms in the proposed energy equations, and an energy budget including potential, zonal, and eddy kinetic energy is derived. This energy budget obtained for the pre-Helene simulated disturbance is discussed in section 6. Additional ideas for improving this energy budget are discussed in section 7. Section 8 gives conclusions and some perspectives on this work.

2. Simulation with Méso-NH

The pre-Helene disturbance was associated with a well-defined AEW and a growing MCS on 9 September 2006 northwest of Burkina Faso (Fig. 1). Successive convective developments associated with the AEW occurred during the two following days. On 12 September, the offshore convective redevelopment south of Cape Verde Islands spawned a tropical depression, which became Hurricane Helene four days later. Following the hypothesis of Berry and Thorncroft (2005) for the case study of Alberto (2000), the cyclogenesis of Helene (2006) could have resulted from the interaction between an AEW and MCSs.

To further investigate the processes involved in this cyclogenesis, a 4-day Méso-NH simulation, starting at 0000 UTC 9 September 2006, was conducted. During these four days, the pre-Helene disturbance propagated over about 3000 km in longitude. Because of computer limitations, it was not possible to run a simulation on this domain and for this duration at a resolved convection scale. Hence, we used a single model configuration with a horizontal resolution of 24 km and parameterized shallow and deep convection with the Kain–Fritsch–Bechtold scheme (Kain and Fritsch 1993; Bechtold et al.

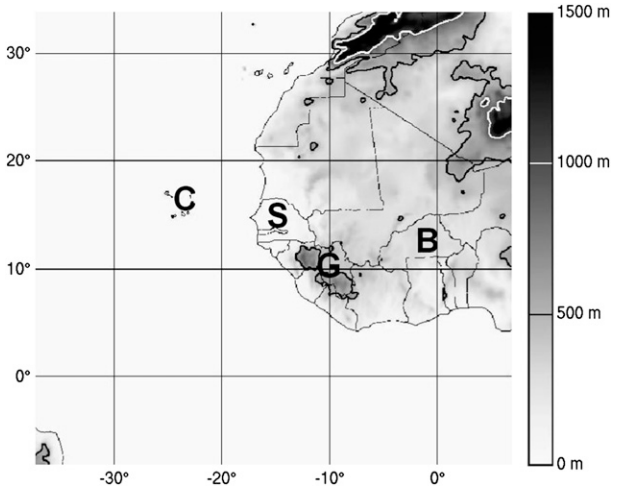

FIG. 1. Terrain elevation in domain of the Méso-NH simulation. The altitude is in meters above mean sea level. Labels indicate locations of West Africa quoted in the text: B = Burkina Faso, C = Cape Verde Islands, G = Guinea Highlands, S = Senegal.

2001). The simulated domain is 4800 km × 4800 km horizontally (Fig. 1). The vertical grid has 66 levels from the surface to 28 km with a grid spacing of 60 m near the surface up to 600 m at the tropopause level, and the orography is taken into account with the Gal-Chen and Sommerville (1975) vertical coordinate. This simulation is coupled with ECMWF operational analyses every 6 h at the boundaries of the simulated domain. Microphysics is parameterized with a one-moment mixed scheme and six classes of liquid and ice hydrometeors (Pinty and Jabouille 1998). Turbulence is parameterized with the 1D scheme with a 1.5-order closure proposed by Bougeault and Lacarrère (1989). Subgrid condensation is represented with the scheme proposed by Chaboureau and Bechtold (2005), and radiative processes with the radiation scheme used at ECMWF (Gregory et al. 2000).

The model outputs are saved every hour. The diagnosed data contain the dynamic and thermodynamic variables as well as the model-derived brightness temperature in the water vapor channel 6 (7.3 μm) of *Meteosat-9* (Saunders et al. 2005; Chaboureau et al. 2000, 2002). The three-dimensional variables are interpolated from the Méso-NH original grid to constant altitude levels to compute the budgets of potential and kinetic energy.

3. Qualitative analysis

The Hovmöller diagram computed with *Meteosat-9* brightness temperature in the water vapor channel 6 (7.3 μm) (Fig. 2a) shows that the pre-Helene disturbance was associated with three convective events: on 10 September over West Africa, on 11 September near the Guinean coast, and on 12 September off shore. The *Meteosat-9* images in Figs. 3a–g allow us to describe this convective activity more precisely. An MCS grew northwest of Burkina Faso on the afternoon of 9 September, propagated westward during the following night and morning, and then dissipated at 1200 UTC 10 September. A squall line developed in front of this system during the afternoon of 10 September, but it quickly dissipated over the Guinean Highlands. An MCS formed behind the previous squall line on 11 September morning, north of the Guinean Highlands, and dissipated over the nearby Atlantic during the afternoon. Finally, an oceanic MCS developed on the morning of 12 September south of Cape Verde Islands, which really started the cyclogenesis of Helene (2006).

The Hovmöller diagram with model-derived brightness temperature (Fig. 2b) shows comparable convective redevelopments, although not exactly at the same times and locations and with slightly warmer brightness temperatures. The model-derived brightness temperature images in Figs. 3h–n display this simulated convective activity more precisely. The MCS starting northwest of Burkina Faso on 9 September is simulated approximately at the right time and location. It spawned another MCS on 10 September afternoon, but this one did not have the shape of a squall line and it dissipated north of the Guinean Highlands during the night of 10 September. Another MCS redeveloped over Dakar (Senegal) on the afternoon of 11 September and intensified gradually. On the afternoon of 12 September, this simulated MCS showed evidence of tropical cyclogenesis (organized convection, cyclonically rotating cloud strips), but it was located about 200 km northeast of the actual MCS at this time. Hence, Méso-NH simulated a comparable but slightly different evolution compared to the actual pre-Helene disturbance. Despite these differences, we consider that a quantitative analysis of the energetic growth of this simulated developing system can provide valuable information on the processes occurring in the real atmosphere.

The Hovmöller diagram of the ECMWF analyzed relative vorticity at 700 hPa (Fig. 2c) shows the zonally moving AEW trough, associated with the previously described convective activity. We therefore suggest the synoptic AEW could have interacted with convection. The Hovmöller diagram of the model-derived relative vorticity at 3000 m (Fig. 2d) shows smaller-scale structures with high values embedded in the cyclonic vorticity zone of the AEW, which might be a consequence of such interactions. Horizontal cross sections of the simulated relative vorticity at 3000 m (Figs. 3o–u) reveal small-scale cyclonic vortices, probably of convective origin,

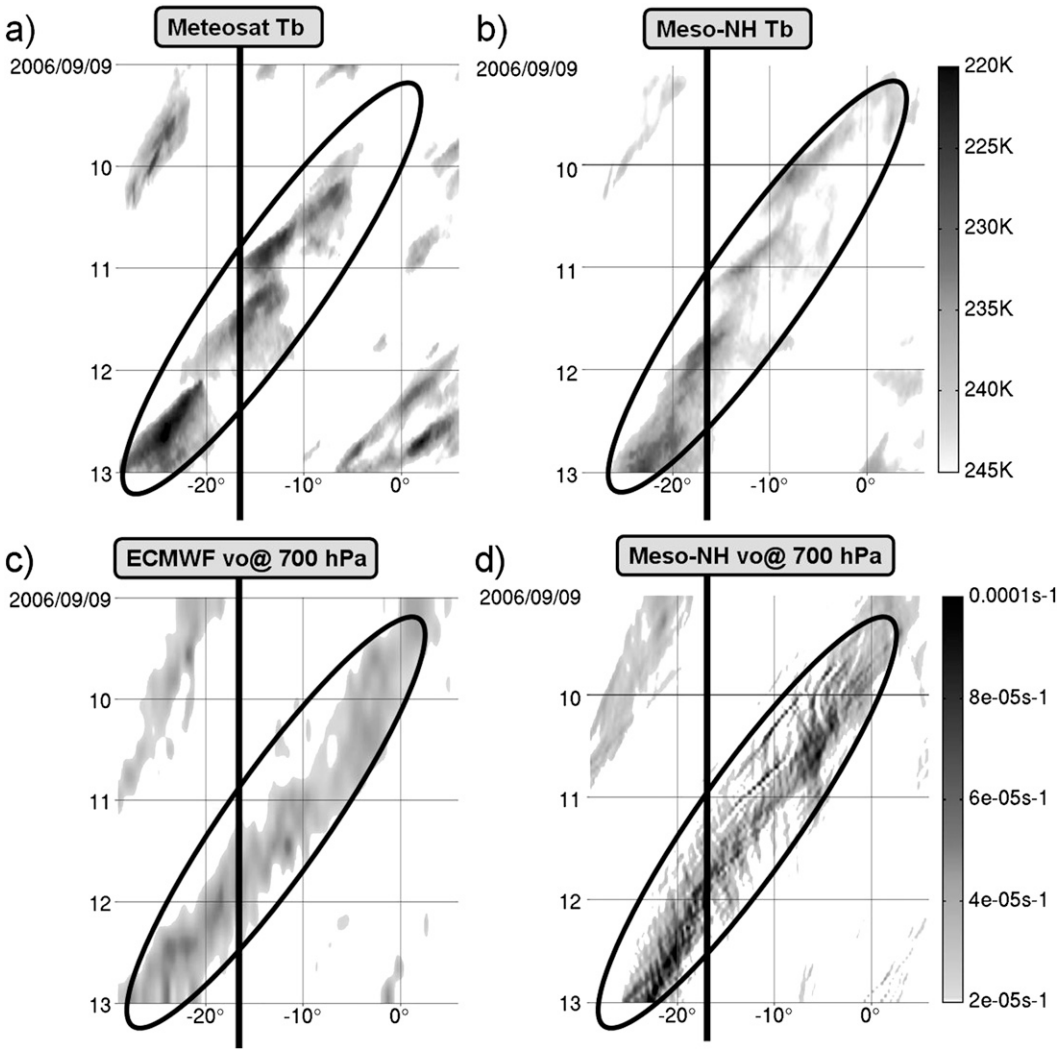

FIG. 2. (a) Hovmöller space–time diagram for *Meteosat-9* brightness temperature (Tb) at 7.3 μm (shaded below 245 K) averaged between 7° and 17°N from 9 to 13 Sep 2006. The horizontal axis indicates longitude in degrees and the vertical axis gives time in days. (b) As in (a) but for model-retrieved brightness temperature. (c) As in (a) but for ECMWF 700-hPa relative vertical vorticity (shaded above $+2 \times 10^5$ s^{-1}). (d) As in (a) except for Méso-NH 3000-m relative vertical vorticity. The gray color scale of brightness temperature (vorticity) is indicated on the top (bottom) right of this figure. In these four diagrams, the vertical line indicates the mean position of the West African coast and the tilted ellipse encloses pre-Helene disturbance.

that merged with the synoptic cyclonic vorticity structure of the AEW, thus intensifying and organizing it, especially near the West African coast. This is consistent with hypothesis of Berry and Thorncroft (2005) that interactions between AEWs and MCSs over the Guinean Highlands play an important role in tropical cyclogenesis off West Africa.

4. Energy budget

Burpee (1972) was the first to apply the L55 energetic analysis to study the growth of AEWs over West Africa. His work was based on 8-yr radiosonde data over the African continent. By evaluating the correlations $[v^*T^*]$ and $[v^*u^*]$ (see the list of symbols in the appendix), he found 1) a sensible heat transport directed down the temperature gradient at each level above the surface, which corresponds to a production of eddy available potential energy by zonal available potential energy, and 2) a horizontal momentum transport with largest magnitude at 700 hPa directed equatorward during the summer season, although the meridional shear of zonal momentum could not be evaluated and the sign of the barotropic conversion between zonal and eddy kinetic

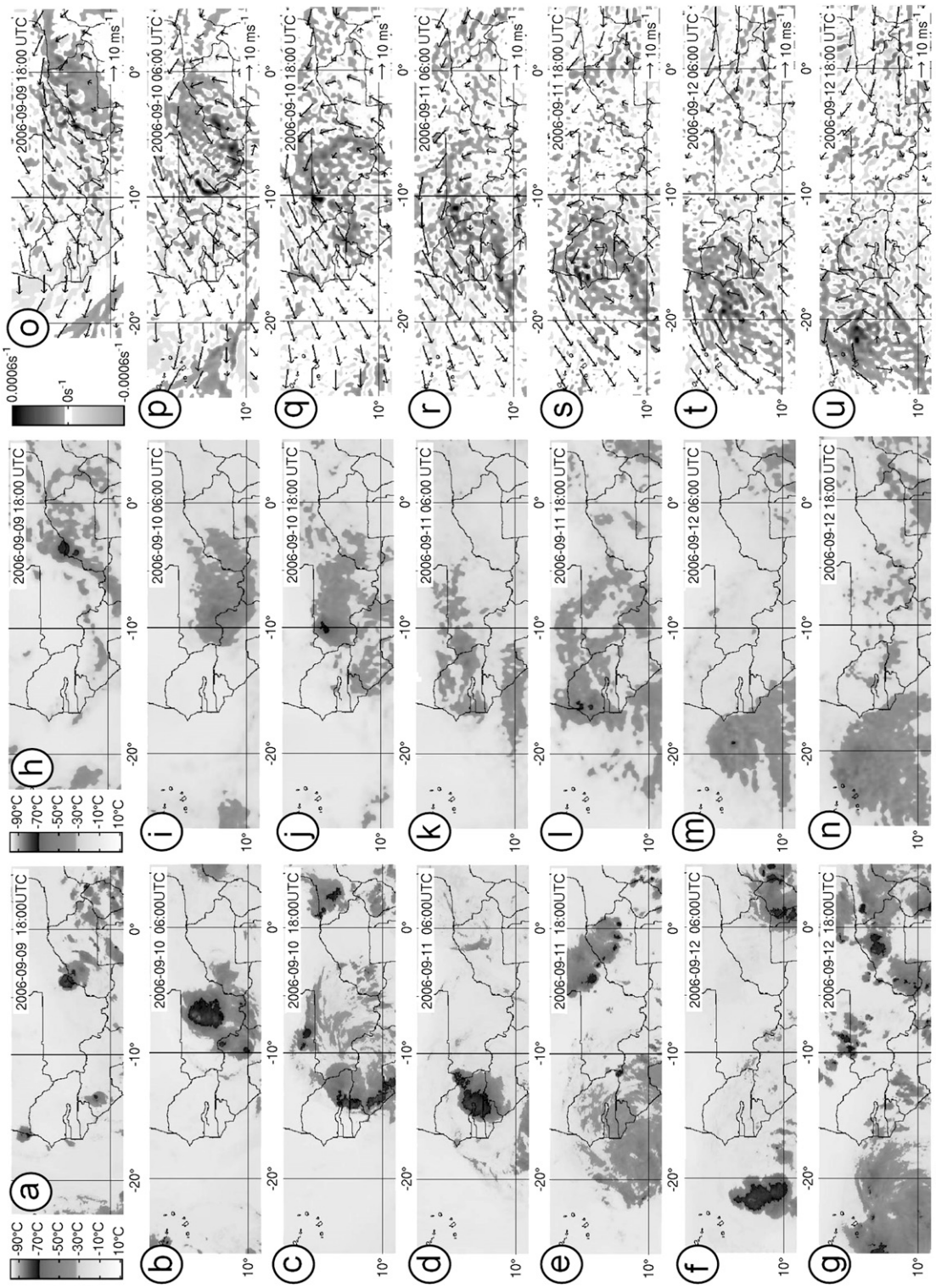

FIG. 3. (a)–(g) Brightness temperature (°C) in the water vapor channel (7.3 μm) derived from *Meteosat-9*; (h)–(n) brightness temperature (°C) in the water vapor channel (7.3 μm) derived from the Méso-NH simulation; (o)–(u) horizontal cross sections of vorticity (s^{-1}) at 3000 m derived from the Méso-NH simulation. These images are from [top; i.e., (a),(h), and (o)] 1800 UTC 9 Sep 2006 until [bottom; i.e., (g),(n), and (u)] 1800 UTC 12 Sep 2006 with a time interval of 12 h.

energy remained undetermined. Moreover, the correlation $[\omega^* T^*]$ could not be evaluated and the baroclinic production of eddy kinetic energy was not quantified in this analysis.

A more complete energy budget was realized by Norquist et al. (1977). Their work was based on the data from the third Global Atmospheric Research Program (GARP) Atlantic Tropical Experiment (GATE III), which was held over West Africa and the eastern tropical Atlantic during the summer of 1974. Their energy budget was done over a limited domain but they neglected the boundary terms, assuming the processes responsible for the growth and/or decay of AEWs occur within their limited domain. They found that the growth of AEWs is both barotropic and baroclinic over West Africa but mostly barotropic over the ocean. This was confirmed by Thompson et al. (1979). Moreover, Norquist et al. (1977) supposed that latent heat released by convective systems over West Africa plays an important role in the baroclinic growth, without quantifying it. In an idealized case study of global circulation, Thorncroft (1995) also suggested that diabatic convective processes participate significantly in the baroclinic growth of AEWs. There was no boundary term in his budget because it was done at global scale. On the contrary, from an idealized case study in a limited domain with moist processes, Paradis et al. (1995) deduced that the baroclinic conversion is mainly compensated by a boundary term representing the redistribution of eddy kinetic energy by the pressure perturbation and that, consequently, it is not associated with production of eddy kinetic energy. Recently, Hsieh and Cook (2007) applied the L55 energetic analysis to a realistic simulation of AEWs during the summer season. They used a wavelet analysis to better understand their evolution. They found that the energy of AEWs over West Africa is mainly maintained by baroclinic conversion and to a smaller extent by barotropic conversion, and that baroclinic growth is sustained mainly by convective heating. Finally, the boundary terms in their budget have a minor contribution and the sink of AEWs' energy is principally due to the frictional dissipation.

These analyses (except Paradis et al. 1995) that are based on the L55 energetic framework confirmed more or less the importance of convective processes in the growth of AEWs. The main problem with the L55 analysis is that it was originally proposed to study the maintenance of the general circulation and as such cannot strictly be applied to a limited domain. Thorncroft (1995), for example, avoids this problem by studying the energetics of a global circulation in an idealized case study. However, this cannot be done for a real case study. Consequently, there is a need to adapt the L55 analysis to a limited domain.

a. Lorenz energetic analysis

Lorenz assumed hydrostatic balance so that pressure can be used as a vertical coordinate, and he neglected the water vapor dependence in the ideal gas constant and in the specific heat of air at constant pressure. L55 showed that the total available potential energy A of the general circulation is proportional to the variance of potential temperature θ [Eq. (8) in L55]:

$$\langle A\rangle = \frac{1}{2} R_a g^{-1} p_{00}^{-\kappa} \int p^{-(1-\kappa)} \left(-\frac{d\langle\theta\rangle}{dp}\right)^{-1} \langle\tilde{\theta}^2\rangle \, dp, \tag{1}$$

where $\langle\cdot\rangle$ denotes integration over the surface of the earth and $\tilde{}$ denotes the departure from this global mean (symbols are explained in the appendix). Using the thermodynamic equation and noting that the net advection term is equal to zero when averaged for the general circulation, the following prognostic equation for $\langle A\rangle$ is obtained [Eq. (16) in L55]:

$$\begin{aligned}\frac{\partial\langle A\rangle}{\partial t} &= g^{-1} R_a \int \frac{\langle\tilde{\omega}\tilde{T}\rangle}{p} \, dp + g^{-1} \int \frac{\langle\tilde{\dot{q}}\tilde{T}\rangle}{c_{pa}\langle\sigma\rangle} \, dp \\ &= -\langle C\rangle + \langle G\rangle,\end{aligned} \tag{2}$$

where $\langle C\rangle$ is the baroclinic conversion term and $\langle G\rangle$ is the diabatic source term. The horizontal kinetic energy $\langle K\rangle$ of the general circulation is defined as [Eq. (11) in L55]

$$\langle K\rangle = \frac{1}{2} g^{-1} \int (\langle u^2 + v^2\rangle) \, dp. \tag{3}$$

With similar arguments, L55 obtained the following prognostic equation for $\langle K\rangle$:

$$\begin{aligned}\frac{\partial\langle K\rangle}{\partial t} &= -g^{-1} \int \left(\left\langle u\frac{\partial\varphi}{\partial x} + v\frac{\partial\varphi}{\partial y}\right\rangle\right) dp \\ &\quad + g^{-1} \int (\langle uF_x + vF_y\rangle) \, dp \\ &= \langle \mathrm{CP}\rangle + \langle D_{\mathrm{friction}}\rangle,\end{aligned} \tag{4}$$

where $\langle \mathrm{CP}\rangle$ is the pressure work and $\langle D_{\mathrm{friction}}\rangle$ is the energy dissipation by friction.

Three remarks can be made: 1) the net advection of geopotential Φ is equal to zero for the general circulation, 2) the vertical gradient of Φ is related to temperature through the hydrostatic equilibrium, and 3) the vertical velocity (ω) in pressure coordinates is equal to

zero when averaged for the general circulation. This leads to another prognostic equation for $\langle K \rangle$ [Eq. (20) in L55]:

$$\frac{\partial \langle K \rangle}{\partial t} = -g^{-1} R_a \int \frac{\langle \tilde{\omega} \tilde{T} \rangle}{p} dp + g^{-1} \int \langle uF_x + vF_y \rangle dp = +\langle C \rangle + \langle D_{\text{friction}} \rangle. \quad (5)$$

From (2) and (5), L55 demonstrated that the so-called ''baroclinic conversion'' $\langle C \rangle$ between $\langle A \rangle$ and $\langle K \rangle$ in the general circulation is proportional to the correlation $\langle \tilde{\omega} \tilde{T} \rangle$. This means that at global scale the ascent of warm air (or descent of cold air) is associated with a decrease of $\langle A \rangle$ and, conversely, an increase of $\langle K \rangle$.

b. Limits of the Lorenz energetic analysis

L55 derived his available potential energy from the total potential energy $\langle E \rangle$ defined as

$$\langle E \rangle = g^{-1} c_{pa} \int \langle T \rangle \, dp; \quad (6)$$

note that E is proportional to the enthalpy ($H = \rho_a c_{pa} T$). In pressure coordinates, the thermodynamic equation is

$$c_{pa} \frac{\partial T}{\partial t} = -c_{pa} \left(u \frac{\partial T}{\partial x} + v \frac{\partial T}{\partial y} + \omega \frac{\partial T}{\partial p} \right) + \frac{R_a \omega T}{p} + \dot{q}. \quad (7)$$

Averaging this equation for the general circulation leads to a prognostic equation for $\langle E \rangle$:

$$\frac{\partial \langle E \rangle}{\partial t} = g^{-1} R_a \int \frac{\langle \tilde{\omega} \tilde{T} \rangle}{p} dp + g^{-1} \int \langle \dot{q} \rangle \, dp = -\langle C \rangle + \langle G \rangle. \quad (8)$$

Equation (8) shows that in the energy budget of the general circulation, the conversion between $\langle E \rangle$ and $\langle K \rangle$ is proportional to the correlation $\langle \tilde{\omega} \tilde{T} \rangle$, so it is equivalent to conversion between $\langle A \rangle$ and $\langle K \rangle$. This equivalence should also be valid at the local scale if A is properly defined, which is not an easy task. We do not follow Marquet (1993, 1995, 2003a) and Shepherd (1993), who tried to define available potential energy as a local quantity. Here, we use the total potential energy E or the enthalpy H in relation with the kinetic energy, and the conversion term between E and K is referred to as the ''horizontal baroclinic conversion.''

By neglecting the pressure tendency in the expression of the vertical velocity ω in pressure coordinates,

$$\omega = u \left(\frac{\partial p}{\partial x} \right)_{y,z} + v \left(\frac{\partial p}{\partial y} \right)_{x,z} + w \left(\frac{\partial p}{\partial z} \right)_{x,y}, \quad (9)$$

neglecting the contribution of water vapor in the equation of state,

$$p = \rho_a R_a T, \quad (10)$$

and approximating the moist air density by the dry air density ρ_a in the definition of Φ in hydrostatic balance,

$$\left(\frac{\partial \varphi}{\partial x} \right)_{y,p} = \frac{1}{\rho_a} \left(\frac{\partial p}{\partial x} \right)_{y,z}, \quad \left(\frac{\partial \varphi}{\partial y} \right)_{x,p} = \frac{1}{\rho_a} \left(\frac{\partial p}{\partial y} \right)_{x,z}, \quad \left(\frac{\partial p}{\partial z} \right)_{x,y} = -\rho_a g, \quad (11)$$

Eq. (7) can be rewritten as

$$c_{pa} \frac{\partial T}{\partial t} = -c_{pa} \left(u \frac{\partial T}{\partial x} + v \frac{\partial T}{\partial y} + \omega \frac{\partial T}{\partial p} \right) + u \left(\frac{\partial \varphi}{\partial x} \right)_{y,p} + v \left(\frac{\partial \varphi}{\partial y} \right)_{x,p} - gw + \dot{q}. \quad (12)$$

Averaging this equation for the general circulation leads to another prognostic equation for $\langle E \rangle$:

$$\frac{\partial \langle E \rangle}{\partial t} = g^{-1} \int \left\langle u \frac{\partial \varphi}{\partial x} + v \frac{\partial \varphi}{\partial y} \right\rangle dp + g^{-1} \int \langle \dot{q} \rangle \, dp = -\langle \text{CP} \rangle + \langle G \rangle. \quad (13)$$

Equations (4) and (13) show that the horizontal baroclinic conversion $\langle \text{CP} \rangle$ between $\langle E \rangle$ and $\langle K \rangle$ is proportional to the horizontal pressure work. It is interesting to note that the horizontal pressure work can only result from the ageostrophic component of the wind. When the circulation is in geostrophic balance and the wind is parallel to the isobars, there is no horizontal baroclinic conversion between E and K.

Marquet (2003b) called the horizontal pressure work the ''ageostrophic conversion term'' and compared it to the baroclinic conversion term of L55 for several case studies in a limited domain. He found that local changes in kinetic energy were directly related to the ageostrophic conversion term, whereas the baroclinic conversion term of L55 was ''out of phase'' and compensated by an additional term: the total (i.e., horizontal plus vertical) work of pressure forces.

The major interest of using CP (i.e., the horizontal pressure work) as the horizontal baroclinic conversion is that it is correct not only at the global scale but also locally, which is not the case for the L55 formulation. When integrating (12) over a limited domain instead of using a global integration, (13) becomes

$$\frac{\partial \overline{E}}{\partial t} = -g^{-1}c_{pa}\int \overline{\left(u\frac{\partial T}{\partial x} + v\frac{\partial T}{\partial y} + \omega\frac{\partial T}{\partial p}\right)}\, dp + g^{-1}\int \overline{\left(u\frac{\partial \varphi}{\partial x} + v\frac{\partial \varphi}{\partial y}\right)}\, dp - \int \overline{w}\, dp + g^{-1}\int \overline{\dot{q}}\, dp = \overline{\mathrm{BE}} - \overline{\mathrm{CP}} - \overline{\mathrm{CVP}} + \overline{G}, \quad (14)$$

where the overbar denotes a horizontal integration over the considered domain and the prime denotes a departure from the horizontal average; $\overline{\mathrm{BE}}$ is the boundary term and $\overline{\mathrm{CVP}}$ is the vertical pressure work. Likewise, integrating (7) over a limited domain gives

$$\frac{\partial \overline{E}}{\partial t} = -g^{-1}c_{pa}\int \overline{\left(u\frac{\partial T}{\partial x} + v\frac{\partial T}{\partial y} + \omega\frac{\partial T}{\partial p}\right)}\, dp + g^{-1}R_a\int \frac{\overline{\omega' T'}}{p}\, dp + g^{-1}R_a\int \frac{\bar{\omega}\overline{T}}{p}\, dp + g^{-1}\int \overline{\dot{q}}\, dp = \overline{\mathrm{BE}} - \overline{C} - \overline{C'} + \overline{G}, \quad (15)$$

where $\overline{C'}$ is a complementary term to account for the nonzero mean vertical velocity.

Similarly, an equation for the evolution of kinetic energy averaged over a limited domain can be derived from (4):

$$\frac{\partial \overline{K}}{\partial t} = -\frac{1}{2}g^{-1}\int \left[\overline{u\frac{\partial (u^2+v^2)}{\partial x} + v\frac{\partial (u^2+v^2)}{\partial y} + \omega\frac{\partial (u^2+v^2)}{\partial p}}\right] dp - g^{-1}\int \overline{\left(u\frac{\partial \varphi}{\partial x} + v\frac{\partial \varphi}{\partial y}\right)}\, dp + g^{-1}\int \overline{(uF_x + vF_y)}\, dp = \overline{\mathrm{BK}} + \overline{\mathrm{CP}} + \overline{D_{\mathrm{friction}}}. \quad (16)$$

In (14), (15), and (16), $\overline{\mathrm{BE}}$ and $\overline{\mathrm{BK}}$ are the boundary terms, which are equal to zero only when averaged over the globe; also, $\overline{\mathrm{CP}}$ in (14) and (16) shows that the horizontal baroclinic conversion between $\overline{E}$ and $\overline{K}$ is still proportional to the horizontal pressure work when the energy budget is limited to a finite domain. On the contrary, a comparison between (14) and (15) reveals that in this case the sum of the baroclinic conversion term $\overline{C}$ proposed by L55 plus another term $\overline{C'}$ in (15) is equal to the sum of two other terms in (14): the horizontal pressure work $\overline{\mathrm{CP}}$ and the vertical pressure work $\overline{\mathrm{CVP}}$. However, without other assumptions, it is not possible to suppose that terms [$\overline{C}$, $\overline{C'}$] and [$\overline{\mathrm{CP}}$, $\overline{\mathrm{CVP}}$] are respectively equal. Therefore, when considering the energy budget over a limited domain, the correlation $\overline{\omega' T'}$ does not strictly correspond to the horizontal baroclinic conversion rate between $\overline{E}$ and $\overline{K}$. This implies that the L55 analysis cannot be directly applied to study the energy budget of a meteorological disturbance (e.g., an AEW) in a limited domain.

c. *Energetic analysis including the vertical pressure work*

The vertical pressure work CVP in (14) is also a source term in the equation of vertical kinetic energy, although it is not possible to write a budget of vertical kinetic energy in hydrostatic balance, as supposed in L55. Thus, we developed a more general energy budget taking into account the vertical kinetic energy, based on the nonhydrostatic, compressible equations given by Bannon (2002).

We use the equation of state of moist air in its original formulation:

$$p = \rho_a R_m T. \quad (17)$$

The conservation equation for the dry air mass used by Bannon (2002) is

$$\frac{\partial \rho_a}{\partial t} + \nabla\cdot(\rho_a \mathbf{u}) = 0. \quad (18)$$

However, the atmospheric gas is a mixture of dry air and water vapor, and it seems more appropriate to consider the density of moist air ρ_m instead of the dry ρ_a, even though it is not a conservative quantity. This is indeed very important for the energetic analysis, given that we have seen in section 4b that the pressure work (linked to pressure gradients) is a measure of the rate of change of potential energy and that both dry air and water vapor actually contribute to the total pressure. From (18) we obtain the following prognostic equation for ρ_m:

$$\frac{\partial \rho_m}{\partial t} = -\nabla\cdot(\rho_m \mathbf{u}) + \rho_a \frac{Dr_v}{Dt}. \quad (19)$$

In (19), the tendency of ρ_m is equal to the sum of its flux divergence plus a term quantifying the variation of mass of moist air due to changes in the water vapor content.

Introducing (19) in the momentum equation of Bannon (2002), we obtain

$$\underbrace{\frac{\partial \rho_m u}{\partial t}}_{\text{(a1)}} = \underbrace{-\nabla\cdot(\rho_m u\mathbf{u})}_{\text{(a2)}} - \underbrace{\frac{\partial p}{\partial x}}_{\text{(a3)}} + \underbrace{\rho_m 2\Omega\ \sin\phi v - \rho_m 2\Omega\ \cos\phi w}_{\text{(a4)}} + \underbrace{\rho_m F_x}_{\text{(a5)}} + \underbrace{\rho_a \dot{u}_{\text{hydro}}}_{\text{(a6)}} + \underbrace{\rho_a u \frac{Dr_v}{Dt}}_{\text{(a7)}}, \tag{20}$$

$$\underbrace{\frac{\partial \rho_m v}{\partial t}}_{\text{(b1)}} = \underbrace{-\nabla\cdot(\rho_m v\mathbf{u})}_{\text{(b2)}} - \underbrace{\frac{\partial p}{\partial y}}_{\text{(b3)}} - \underbrace{\rho_m 2\Omega\ \sin\phi u}_{\text{(b4)}} + \underbrace{\rho_m F_y}_{\text{(b5)}} + \underbrace{\rho_a \dot{v}_{\text{hydro}}}_{\text{(b6)}} + \underbrace{\rho_a v \frac{Dr_v}{Dt}}_{\text{(b7)}}, \tag{21}$$

$$\underbrace{\frac{\partial \rho_m w}{\partial t}}_{\text{(c1)}} = \underbrace{-\nabla\cdot(\rho_m w\mathbf{u})}_{\text{(c2)}} - \underbrace{\frac{\partial p}{\partial z}}_{\text{(c3)}} + \underbrace{\rho_m 2\Omega\ \cos\phi u}_{\text{(c4)}} + \underbrace{\rho_m F_z}_{\text{(c5)}} + \underbrace{\rho_a \dot{w}_{\text{hydro}}}_{\text{(c6)}} + \underbrace{\rho_a w \frac{Dr_v}{Dt}}_{\text{(c7)}} - \underbrace{\rho_m g}_{\text{(c8)}}. \tag{22}$$

In (20), (21), and (22), the terms related to the earth's curvature have been neglected; (a1), (b1), (c1) and (a2), (b2), and (c2) are the tendencies and flux divergences of moist momentum, respectively; (a3), (b3), and (c3) are the components of the pressure force; (a4), (b4), and (c4) the components of the Coriolis force; (a5), (b5), and (c5) the components of the frictional force; (a6), (b6), and (c6) the approximated momentum forcing of the moist air by the hydrometeors; (a7), (b7), and (c7) the variation of moist momentum due to variations of water vapor content; and (c8) is the gravitational force.

Using (20), (21), and (22), we find two prognostic equations for the horizontal kinetic energy $K^C = \frac{1}{2}\rho_m(u^2 + v^2)$ and the vertical kinetic energy $\mathrm{KV}^C = \frac{1}{2}\rho_m w^2$:

$$\frac{\partial K^C}{\partial t} = -\nabla\cdot(K^C\mathbf{u}) - \left(u\frac{\partial p}{\partial x} + v\frac{\partial p}{\partial y}\right) - \rho_m 2\Omega\ \cos\phi wu + \rho_m(uF_x + vF_y) + \rho_a(u\dot{u}_{\text{hydro}} + v\dot{v}_{\text{hydro}}) + \rho_a\frac{u^2+v^2}{2}\frac{Dr_v}{Dt}$$
$$= \mathrm{BK}^C + \mathrm{CP}^C - \mathrm{CC}^C + D^C_{\text{friction}} + D^C_{\text{hydro}} + D^C_{\text{wv}}. \tag{23}$$

$$\frac{\partial \mathrm{KV}^C}{\partial t} = -\nabla\cdot(\mathrm{KV}^C\mathbf{u}) - w\frac{\partial p}{\partial z} + \rho_m 2\Omega\ \cos\phi wu - \rho_m gw + \rho_m wF_z + \rho_a\dot{w}_{\text{hydro}}w + \rho_a\frac{w^2}{2}\frac{Dr_v}{Dt}$$
$$= \mathrm{BKV}^C + \mathrm{CVP}^C + \mathrm{CC}^C + \mathrm{DV}^C_{\text{gravity}} + \mathrm{DV}^C_{\text{friction}} + \mathrm{DV}^C_{\text{hydro}} + \mathrm{DV}^C_{\text{wv}}. \tag{24}$$

In (23), the tendency of K^C is equal to the sum of flux divergence BK^C and source terms: the horizontal pressure work CP^C; the partial work of the Coriolis force CC^C, which corresponds to a conversion between K^C and KV^C; the horizontal work of friction D^C_{friction}; the horizontal work of the momentum forcing of moist air by the hydrometeors D^C_{hydro}; and the variation of K^C due to variations of the water vapor content D^C_{wv}. In (24), the tendency of KV^C is equal to the sum of the flux divergence BKV^C and the source terms: the vertical pressure work CVP^C, the partial work of the Coriolis force CC^C, the work of the gravitational force $\mathrm{DV}^C_{\text{gravity}}$, the vertical frictional work $\mathrm{DV}^C_{\text{friction}}$, the vertical work of the momentum forcing of moist air by the hydrometeors $\mathrm{DV}^C_{\text{hydro}}$, and the variation of KV^C due to variations of water vapor content $\mathrm{DV}^C_{\text{wv}}$.

With a similar rearrangement, and introducing the moist enthalpy ($H^C_m = \rho_a c_{pm} T$), the thermodynamic equation of Bannon (2002) becomes

$$\frac{\partial H^C_m}{\partial t} = -\nabla\cdot(H^C_m\mathbf{u}) + \frac{\partial p}{\partial t} + \left(u\frac{\partial p}{\partial x} + v\frac{\partial p}{\partial y} + w\frac{\partial p}{\partial z}\right) + \rho_a\dot{q}_{\text{phase}} + \rho_a\dot{q}_{\text{diab}} - (r_l\rho_a\dot{q}_l + r_i\rho_a\dot{q}_i) + \rho_a c_{pv}T\frac{Dr_v}{Dt}$$
$$= \mathrm{BH}^C + G^C_p - (\mathrm{CP}^C + \mathrm{CPV}^C) + G^C_{\text{phase}} + G^C_{\text{diab}} + G^C_{\text{hydro}} + G^C_{\text{wv}}. \tag{25}$$

In (25), the tendency of H_m^C is equal to the sum of flux divergence BH^C and source terms: the pressure tendency G_p^C; the total pressure work ($\mathrm{CP}^C + \mathrm{CPV}^C$); the term associated with changes of water phase G_{phase}^C; the heating rate due to other diabatic processes (e.g., radiative heating and turbulent dissipation) G_{diab}^C; the opposite of the total heating rate of hydrometeors G_{hydro}^C (this term appears because we consider the variation of moist enthalpy only, without including the contribution of hydrometeors); and the variation of H_m^C due to variations of water vapor content G_{wv}^C.

Equations (23), (24), and (25) show that H_m^C can be converted into (produced by) horizontal and/or vertical kinetic energy through the horizontal CP^C and vertical CVP^C baroclinic conversions, the sum of these terms being equal to the total pressure work. This is a generalization of the result found in section 4b. When integrated over a spatial (finite or global) domain, (23), (24), and (25) constitute an energy budget including moist enthalpy and horizontal and vertical kinetic energies, schematically displayed in Fig. 4.

d. Energetic analysis including the anelastic approximation

The Méso-NH model uses a moist version of Durran's (1989) anelastic equations, so the energy analysis of section 4c must be adapted before applying it to the simulation results. In Méso-NH, the anelastic version of moist momentum equations, which includes the dry air density of the reference state $\rho_{a\mathrm{ref}}$, is

$$\underbrace{\frac{\partial(1+r_v)\rho_{a\mathrm{ref}}u}{\partial t}}_{\text{(d1)}} = \underbrace{-\nabla\cdot[(1+r_v)\rho_{a\mathrm{ref}}u\mathbf{u}]}_{\text{(d2)}} \underbrace{-\frac{(1+r_v)\rho_{a\mathrm{ref}}}{(1+r_v+r_{\mathrm{hydro}})\rho_a}\frac{\partial p}{\partial x}}_{\text{(d3)}} \underbrace{+(1+r_v)\rho_{a\mathrm{ref}}[2\Omega\ \sin\phi v - 2\Omega\ \cos\phi w_a]}_{\text{(d4)}}$$
$$+\underbrace{(1+r_v)\rho_{a\mathrm{ref}}F_x}_{\text{(d5)}} + \underbrace{\rho_{a\mathrm{ref}}u\frac{Dr_v}{Dt}}_{\text{(d6)}}, \tag{26}$$

$$\underbrace{\frac{\partial(1+r_v)\rho_{a\mathrm{ref}}v}{\partial t}}_{\text{(e1)}} = \underbrace{-\nabla\cdot[(1+r_v)\rho_{a\mathrm{ref}}v\mathbf{u}]}_{\text{(e2)}} \underbrace{-\frac{(1+r_v)\rho_{a\mathrm{ref}}}{(1+r_v+r_{\mathrm{hydro}})\rho_a}\frac{\partial p}{\partial y}}_{\text{(e3)}} \underbrace{-(1+r_v)\rho_{a\mathrm{ref}}2\Omega\ \sin\phi u}_{\text{(e4)}}$$
$$+\underbrace{(1+r_v)\rho_{a\mathrm{ref}}F_y}_{\text{(e5)}} + \underbrace{\rho_{a\mathrm{ref}}v\frac{Dr_v}{Dt}}_{\text{(e6)}}, \tag{27}$$

$$\underbrace{\frac{\partial(1+r_v)\rho_{a\mathrm{ref}}w}{\partial t}}_{\text{(f1)}} = \underbrace{-\nabla\cdot[(1+r_v)\rho_{a\mathrm{ref}}w\mathbf{u}]}_{\text{(f2)}} \underbrace{-\frac{(1+r_v)\rho_{a\mathrm{ref}}}{(1+r_v+r_{\mathrm{hydro}})\rho_a}\frac{\partial p}{\partial z}}_{\text{(f3)}} \underbrace{+(1+r_v)\rho_{a\mathrm{ref}}2\Omega\ \cos\phi u}_{\text{(f4)}}$$
$$+\underbrace{(1+r_v)\rho_{a\mathrm{ref}}F_z}_{\text{(f5)}} + \underbrace{\rho_{a\mathrm{ref}}w\frac{Dr_v}{Dt}}_{\text{(f6)}} \underbrace{-(1+r_v)\rho_{a\mathrm{ref}}g}_{\text{(f7)}}. \tag{28}$$

In (26), (27), and (28), terms (d1), (e1), and (f1) are tendencies; (d2), (e2), and (f2) flux divergences; and (d3), (e3), and (f3) the components of the pressure force. These pressure force components include the mixing ratio of hydrometeors ($r_{\mathrm{hydro}} = r_l + r_i$) because they have been written with the moist air density, which includes hydrometeors. At first order, development of r_{hydro} allows us to separate the contribution of hydrometeors in the pressure terms. The terms (d4), (e4), and (f4) are the components of the Coriolis force; (d5), (e5), and (f5) the components of the frictional force; (d6), (e6), and (f6) the variation of the anelastic version of moist momentum due to variations of water vapor content; and (f7) is the gravitational force.

From (26), (27), and (28), we obtain two prognostic equations for the anelastic formulation of horizontal kinetic energy $K^A = \frac{1}{2}(1 + r_v)\rho_{a\mathrm{ref}}(u^2 + v^2)$ and vertical kinetic energy $\mathrm{KV}^A = \frac{1}{2}(1 + r_v)\rho_{a\mathrm{ref}}w^2$:

$$\frac{\partial K^A}{\partial t} = -\nabla\cdot(K^A\mathbf{u}) - \frac{\rho_{a\mathrm{ref}}}{\rho_a}\left(u\frac{\partial p}{\partial x} + v\frac{\partial p}{\partial y}\right) - (1+r_v)\rho_{a\mathrm{ref}}2\Omega\ \cos\phi wu + (1+r_v)\rho_{a\mathrm{ref}}(uF_x + vF_y)$$
$$+ r_{\mathrm{hydro}}\frac{\rho_{a\mathrm{ref}}}{\rho_a}\left(u\frac{\partial p}{\partial x} + v\frac{\partial p}{\partial y}\right) + \rho_{a\mathrm{ref}}\frac{u^2+v^2}{2}\frac{Dr_v}{Dt}$$
$$= \mathrm{BK}^A + \mathrm{CP}^A - \mathrm{CC}^A + D^A_{\mathrm{friction}} + D^A_{\mathrm{hydro}} + D^A_{\mathrm{wv}}, \tag{29}$$

$$\frac{\partial \mathrm{KV}^A}{\partial t} = -\nabla\cdot(\mathrm{KV}^A\mathbf{u}) - \frac{\rho_{a\mathrm{ref}}}{\rho_a}w\frac{\partial p}{\partial z} + (1+r_v)\rho_{a\mathrm{ref}}2\Omega\ \cos\phi wu - (1+r_v)\rho_{a\mathrm{ref}}gw + (1+r_v)\rho_{a\mathrm{ref}}wF_z$$
$$+ r_{\mathrm{hydro}}\frac{\rho_{a\mathrm{ref}}}{\rho_a}w\frac{\partial p}{\partial z} + \rho_{a\mathrm{ref}}\frac{w^2}{2}\frac{Dr_v}{Dt}$$
$$= \mathrm{BKV}^A + \mathrm{CPV}^A + \mathrm{CC}^A + \mathrm{DV}^A_{\mathrm{gravity}} + \mathrm{DV}^A_{\mathrm{friction}} + \mathrm{DV}^A_{\mathrm{hydro}} + \mathrm{DV}^A_{\mathrm{wv}}. \tag{30}$$

Although they are written differently, the same terms appear in (29) and (30) that appeared earlier in (23) and (24), respectively.

The anelastic thermodynamic equation used in Méso-NH is

$$\frac{D\theta}{Dt} = \underbrace{\frac{\dot q_{\mathrm{phase}} + \dot q_{\mathrm{diab}}}{\pi_{\mathrm{ref}}(c_{pm} + c_{\mathrm{hydro}})}}_{\text{(a)}} + \underbrace{\left(\frac{R_m}{c_{pm}+c_{\mathrm{hydro}}}\frac{c_{pa}}{R_a} - 1\right)\frac{\theta}{\pi_{\mathrm{ref}}}\frac{D\pi_{\mathrm{ref}}}{Dt}}_{\text{(b)}}, \tag{31}$$

where π_{ref} is the Exner function of the reference state and $c_{\mathrm{hydro}} = r_l c_l + r_i c_i$, where $r_l(r_i)$ and $c_l(c_i)$ are the mixing ratio and specific heat of liquid water (ice). In (31), term (a) is proportional to the diabatic heating rate, and term (b) corresponds to the moist correction in absence of any phase change. Using (25) and (31), the equation for the moist enthalpy can be written as

$$\frac{\partial H^C_m}{\partial t} = -\nabla\cdot(H^A_m\mathbf{u}) + \frac{\rho_{a\mathrm{ref}}}{\rho_a}\frac{\partial p}{\partial t} + \frac{\rho_{a\mathrm{ref}}}{\rho_a}\left(u\frac{\partial p}{\partial x} + v\frac{\partial p}{\partial y} + w\frac{\partial p}{\partial z}\right) + \left(\frac{p}{p_{\mathrm{ref}}}\right)^{\kappa}\rho_{a\mathrm{ref}}\dot q_{\mathrm{phase}} + \left(\frac{p}{p_{\mathrm{ref}}}\right)^{\kappa}\rho_{a\mathrm{ref}}\dot q_{\mathrm{diab}}$$
$$- \rho_{a\mathrm{ref}}c_{\mathrm{hydro}}\frac{DT}{Dt} + \rho_{a\mathrm{ref}}c_{pv}T\frac{Dr_v}{Dt} + \frac{\rho_{a\mathrm{ref}}}{\rho_a}\left(1 - \frac{c_{pm}+c_{\mathrm{hydro}}}{c_{pa}}\frac{R_a}{R_m}\right)\left(\frac{p}{p_{\mathrm{ref}}}\frac{Dp_{\mathrm{ref}}}{Dt} - \frac{Dp}{Dt}\right)$$
$$= \mathrm{BH}^A + G^A_P - (\mathrm{CP}^A + \mathrm{CPV}^A) + G^A_{\mathrm{phase}} + G^A_{\mathrm{diab}} + G^A_{\mathrm{hydro}} + G^A_{\mathrm{wv}} + G^A_{\mathrm{residual}}, \tag{32}$$

where p_{ref} is the pressure of the reference state. Although they are written differently, the same terms appear in (25) and (32). The additional term G^A_{residual} in (32) is due to the fact that the thermodynamic Eq. (31) is written with the dry potential temperature and that the pressure of the reference state p_{ref} is used in the moist correction term. The fact that CP^A and CVP^A appear in (29), (30), and (32) implies that the horizontal (vertical) baroclinic conversion between H^A_m and K^A (KV^A) is correctly described with this set of anelastic equations. Hence, when integrated over the spatial (global or finite) domain, (29), (30), and (32) constitute an energetic budget encompassing anelastic versions of moist enthalpy and horizontal and vertical kinetic energies. For simplicity, the superscript A's are omitted hereafter.

5. Application and scale analysis

The energy budget presented in section 4d is applied to the results of the Méso-NH simulation of the pre-Helene disturbance within domain D defined as 9°–18°N, 26°W–5°E horizontally (see Fig. 3) and 1000–18 000 m above mean sea level. Then, the terms BK, BKV, and BH of (30), (31), and (32) are boundary terms that represent the contribution of energy exchanges between atmospheric flows inside and outside domain D.

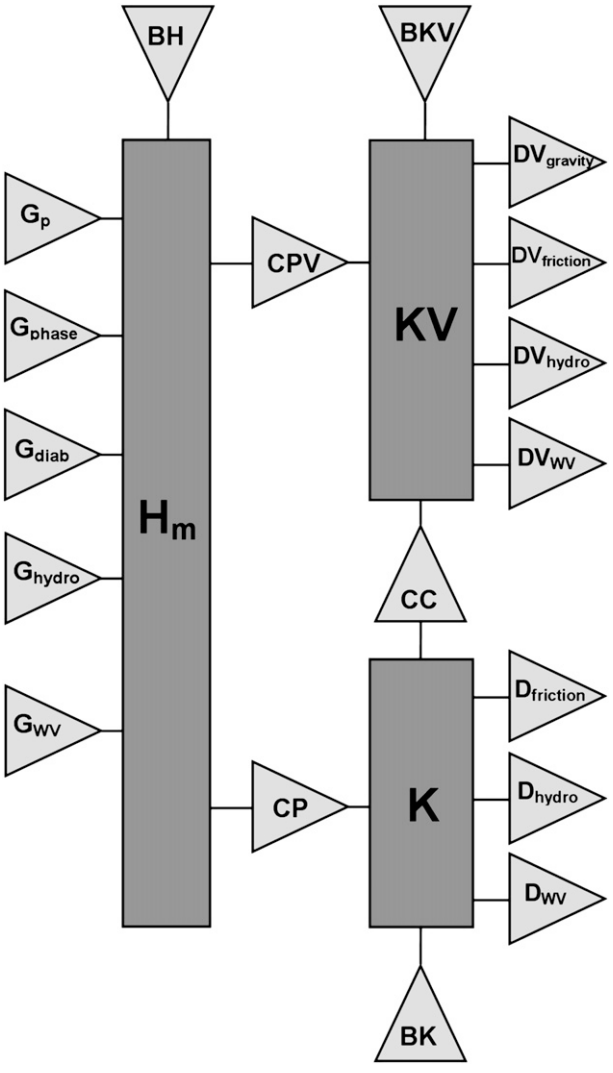

FIG. 4. Schematic view of the energy budget proposed in section 4c. The mathematical expression and significance of the energies (H_m, K, KV), boundary terms (BH, BK, BKV), conversion terms (CP, CPV, CC) and source/sink terms [G_p, G_{phase}, G_{diab}, G_{hydro}, G_{wv} for moist enthalpy; $\text{DV}_{\text{gravity}}$, $\text{D(V)}_{\text{friction}}$, $\text{D(V)}_{\text{hydro}}$, D(V)_{wv} for horizontal/vertical kinetic energy] are given in the text.

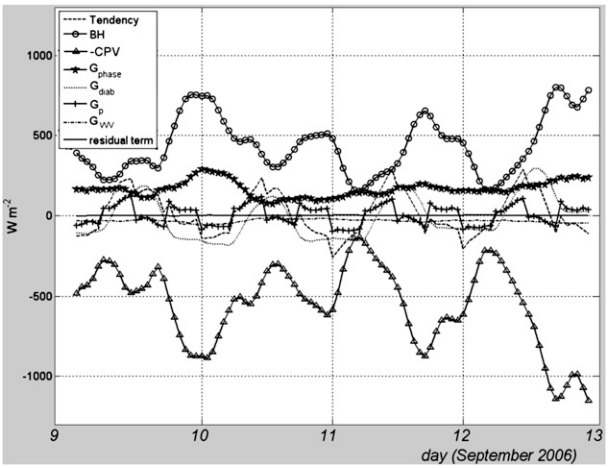

FIG. 5. First-order terms in the budget of H_m for the simulated pre-Helene disturbance, averaged over horizontal domain D and between altitudes 1000 and 18 000 m. The horizontal axis gives the time in days from 0000 UTC 9 Sep 2006. The vertical axis gives the intensity in W m^{-2}. The coefficients displayed are the tendency of H_m (dashed line); BH (solid line with circles); the opposite of CPV (solid line with triangles); G_{phase} (solid line with stars); G_{diab} (dotted line); G_p (solid line with plus signs); G_{wv} (dashed–dotted line); and the first-order residual term (solid line).

a. Budget of moist enthalpy

The budget of H_m [Eq. (32); Figs. 5 and 6] is nearly balanced by seven ''first-order'' terms referred to as ''primary processes'' ($<\pm 0.1$ W m^{-3} in Fig. 6). The evolution of H_m is characterized by a diurnal cycle with positive tendencies during the day and negative ones during the night, between the surface and 12 000 m. This diurnal cycle is mostly forced by radiative heating G_{diab}, with some influence of the semidiurnal variation of G_P, in relation to the atmospheric tide (e.g., Dai and Wang 1999) and the coupling with the ECMWF analyses every 6 h. In domain D, the mean vertical velocity is always positive owing to convective and radiative processes with larger values during evening, as can be deduced from Fig. 6c showing positive values of CPV, proportional to $(-w\partial p/\partial z)$, with p decreasing with height. The boundary term BH is dominated by the vertical flux divergence $[-\partial(Hw)/\partial z]$, which is positive because w is positive and H decreases with height. This means that in this modeled case study, the production of moist enthalpy by diabatic processes, including radiation and latent heat release, is mostly dissipated by a direct vertical baroclinic conversion (CPV > 0).

The term G_{wv}, related to humidity changes, is mainly negative, which is coherent with water vapor globally condensing within the domain ($G_{\text{phase}} > 0$). The diurnal positive values of G_{wv} at low levels correspond to surface evaporation at the hottest time of the day. They are associated with negative values of G_{phase} and enhanced positive values of G_{diab} (see Figs. 6d,e,g).

The budget of H_m also involves two ''second-order'' terms referred to as ''secondary processes'' ($<\pm 10^{-3}$ W m^{-3} in Fig. 7). One of them is the generation of moist enthalpy by hydrometeors G_{hydro}, which mostly results from the upward transport of nonprecipitating liquid and ice particles that carry sensible heat from lower levels and transmit it to the colder air above. It can be noted that the maximum of G_{hydro} during the night of 9–10 September is correlated with the maximum of G_{phase}, associated with strong convective activity. The other secondary process is the horizontal baroclinic conversion

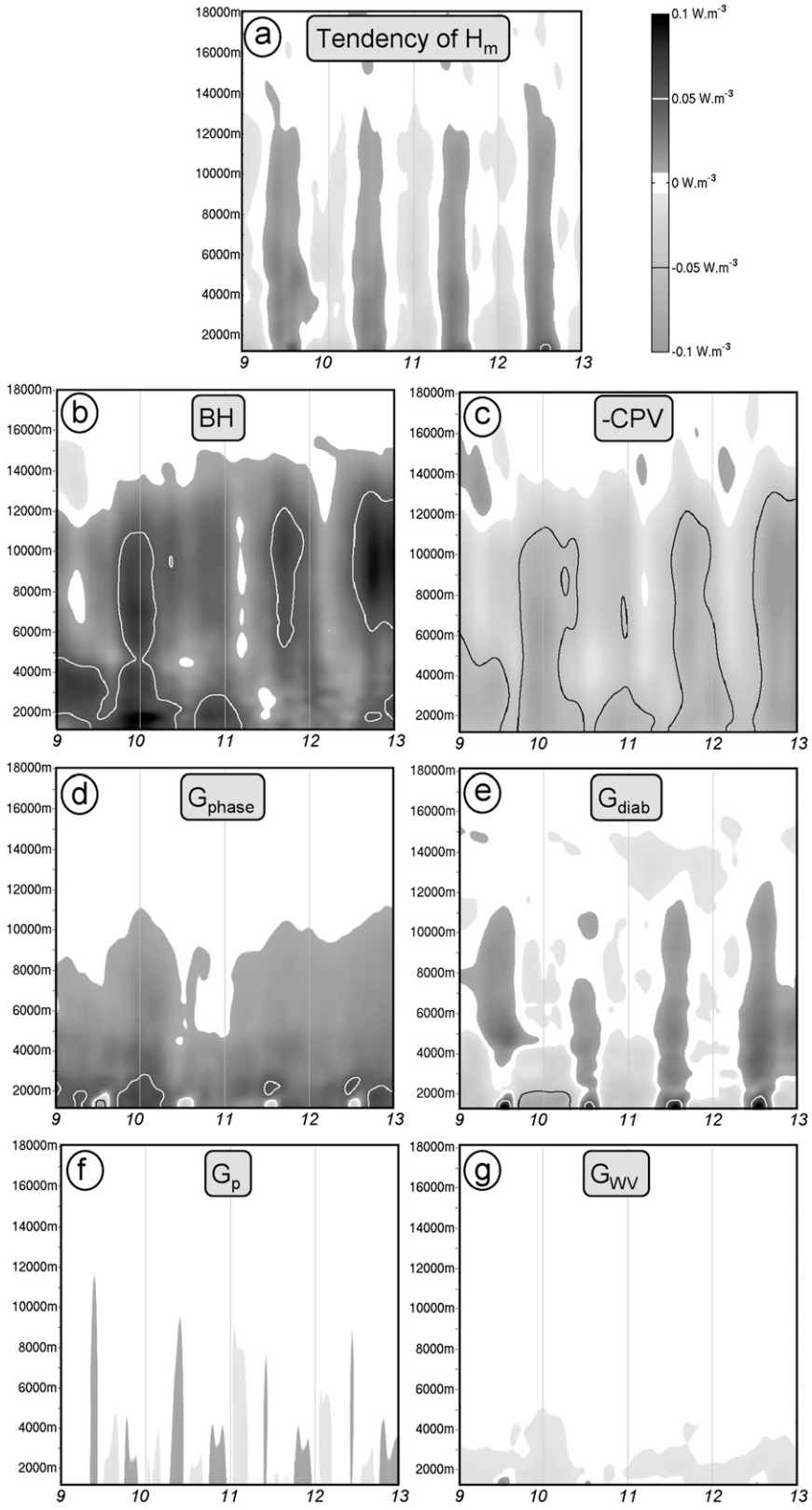

FIG. 6. Time–altitude plots of the first-order terms in the budget of H_m. The horizontal axis gives the time in days from 0000 UTC 9 Sep 2006 to 0000 UTC 12 Sep 2006. The vertical axis gives the altitude (m). These terms are in W m^{-3} and the gray color scale is indicated in the upper right.

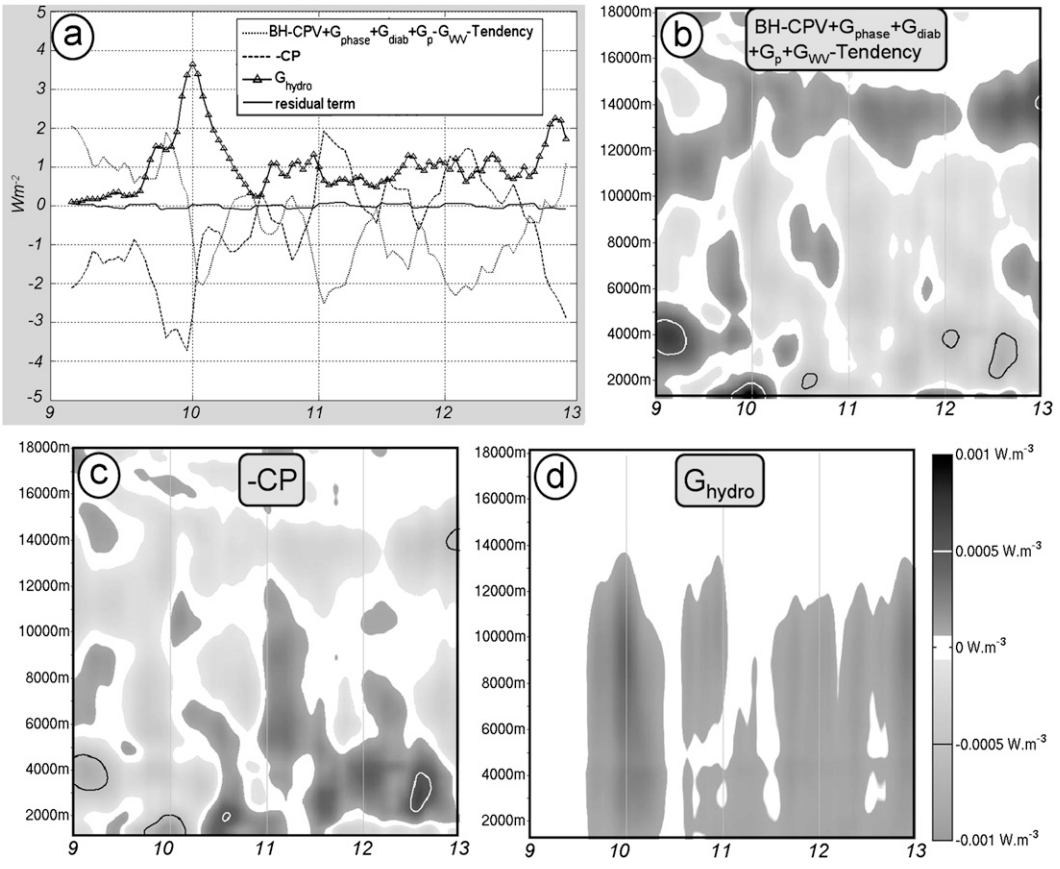

FIG. 7. (a) As in Fig. 5, but for the second-order terms in the budget of H_m. The coefficients displayed are the residual term of the first-order terms (dotted line); CP (dashed line); G_{hydro} (solid line with triangles); and the second-order residual term of this budget (solid line). (b)–(d) As in Fig. 6, but for the second-order terms in the budget of H_m.

term CP with two periods with positive values ($-\text{CP} < 0$ in Fig. 7c) on 9 and late 12 September, during which energy is transferred from the moist enthalpy to the kinetic energy through a direct horizontal baroclinic conversion, and a period of negative values ($-\text{CP} > 0$ in Fig. 7c) during 10–12 September, during which energy is transferred from the kinetic energy to the moist enthalpy through an inverse horizontal baroclinic conversion. An analysis of the associated physical processes is given below.

The additional term G_{residual} (not shown) in the budget of H_m is negligible compared to the other ones presented above. Its amplitude is about 50 times smaller ($<\pm 2\ 10^{-5}$ W m^{-3}) than the secondary terms displayed in Fig. 7. This result gives us confidence in the accuracy of the anelastic approximation of Méso-NH in terms of energy conservation.

b. Budget of horizontal kinetic energy

The budget of K [Eq. (29)] is approximately balanced at first order by three primary processes ($<\pm 10^{-3}$ W m^{-3} in Fig. 8). The horizontal kinetic energy increases on 9 September and partly on 10 September, decreases on the 11th and 12th, and then increases again during the evening of the 12th. This evolution is apparently controlled by the horizontal baroclinic conversion CP, with some influence from the negative friction term D_{friction} and from the positive advection term BK in the low to mid levels.

The first-order residual of the kinetic energy budget is almost balanced by the second-order conversion term CC between horizontal and vertical kinetic energy due to the work of the Coriolis force ($<\pm 0^{-5}$ W m^{-3} in Fig. 9). This term is proportional to $-uw$ and, owing to the mean upward motions, it is negative (positive) in the low (mid to upper) levels because of the presence of southwesterly (easterly) winds. It can be noted that the higher extension of negative values on 10 and 11 September could be related to the upward transport of southwesterly momentum, in conjunction with enhanced convective activity diagnosed by G_{phase} in Fig. 6. The remaining terms—the dissipation of K by condensation/deposition of water vapor D_{wv} and the momentum forcing associated with hydrometeors D_{hydro}—are negligible.

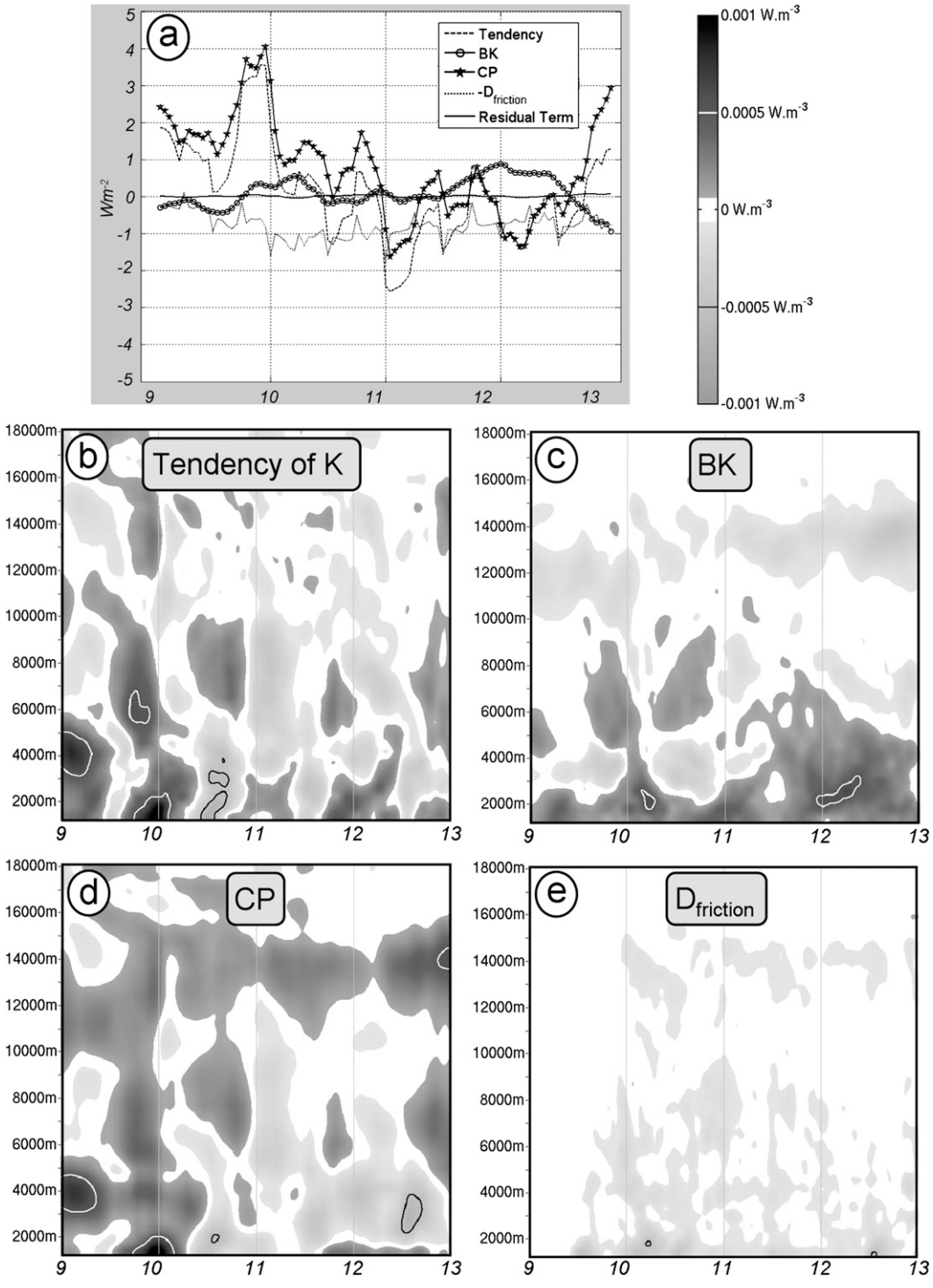

FIG. 8. (a) As in Fig. 5, but for the first-order terms in the budget of K. The displayed coefficients are the tendency of K (dashed line); BK (solid line with circles); CP (solid line with stars); D_{friction} (dotted line); and the first-order residual term of this budget (solid line). (b)–(d) As in Fig. 6, but for the first-order terms in the budget of K.

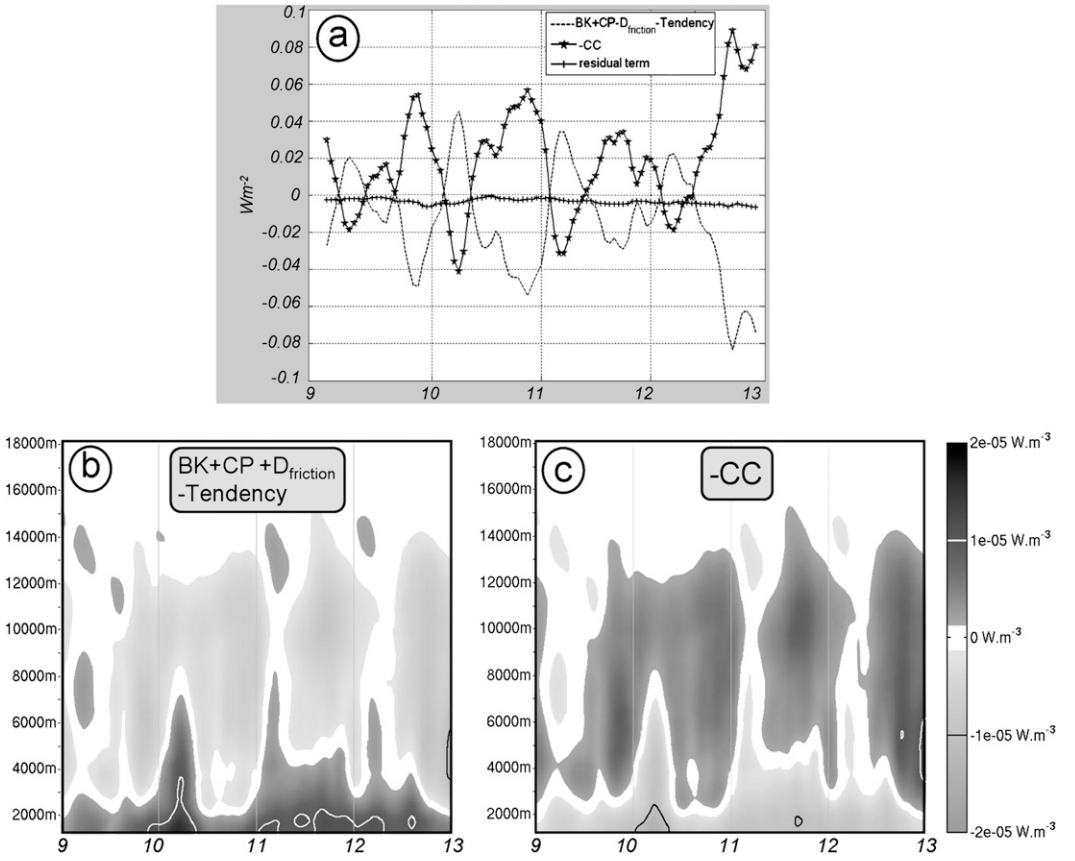

FIG. 9. (a) As in Fig. 5, but for the second-order terms in the budget of K. The displayed coefficients are the residual term of the first-order terms (dashed line); CC (solid line with stars); and the second-order residual term of this budget (solid line with plus signs). (b)–(d) As in Fig. 6, but for the second-order terms in the budget of K.

c. *Budget of vertical kinetic energy*

The budget of KV [Eq. (30)] is characterized by a very weak tendency with a near balance between two first-order terms ($<\pm 0.1$ W m^{-3} in Fig. 10), referred to as primary processes—the vertical baroclinic conversion term CVP and the work of the gravitational force D_{gravity}. It is a well-known result that at first order, changes in potential energy are balanced by the work associated with the vertical displacement of the atmospheric column.

The residual of these first-order terms is mostly balanced by two secondary processes ($<\pm 10^{-3}$ W m^{-3} in Fig. 11): the vertical frictional dissipation $\text{DV}_{\text{friction}}$ and the dissipation by vertical momentum forcing of moist air associated with hydrometeors DV_{hydro}. They have comparable contributions, with the second showing a maximum in relation with convective activity during the night of 9–10 September.

The budget of KV also involves ''third-order'' terms referred to as ''tertiary processes'' ($<\pm 10^{-5}$ W m^{-3} in Fig. 12): the conversion CC between K and KV due to the work of the Coriolis force, the boundary term BKV, and the tendency of KV. The vertically integrated contribution of BKV is negligible as a result of opposing values in the lower and upper troposphere, probably related to a net inflow of ascending air in the low levels and a net outflow of subsiding air in the upper levels. The tendency of KV is small, but not negligible locally. However, it varies rapidly from positive to negative values, and vice versa, so that KV remains close to zero. The vertical dissipation DV_{wv} associated with water vapor condensation and/or deposition of water vapor (not shown) is about two orders of magnitude smaller than the third-order terms in the budget of KV, so it can be neglected.

d. *Synthesis*

Several processes at different orders of magnitude have been described in the energy budgets (see Table 1 for a classification of these processes with respect to their magnitude). In this study, we are concerned with the horizontal kinetic energy of the simulated pre-Helene disturbance, so we only need to consider the primary processes in the budget of K. At this first order of magnitude, the conversion term between K and KV can

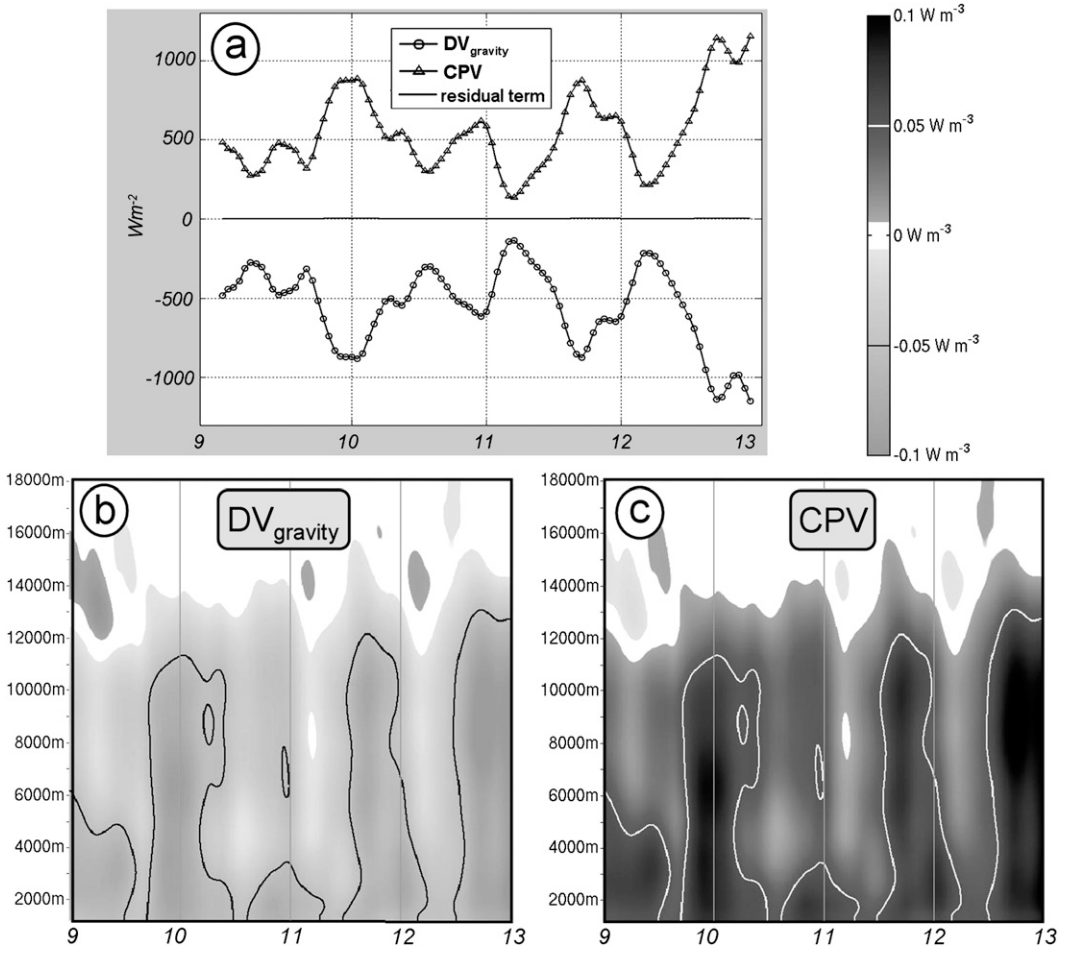

FIG. 10. (a) As in Fig. 5, but for the first-order terms in the budget of KV. The displayed coefficients are $DV_{gravity}$ (solid line with circles); CPV (solid line with triangles); and the first-order residual term of this budget (solid line). (b),(c) As in Fig. 6, but for the first-order terms in the budget of KV.

be neglected, so the budget of KV is disregarded (as well as term CC in the budget of K). Moreover, the vertical baroclinic conversion term CPV can be considered as a ''dissipation'' term in the budget of H_m, in relation with the vertical reorganization of the atmosphere through the work of the gravitational force $DV_{gravity}$. However, CPV cannot be approximated by $-DV_{gravity}$ because CP and the sum CPV + $DV_{gravity}$ have comparable magnitudes. The introduction of water vapor in the boundary terms BK and BH resulted in additional dissipation terms D_{wv} and G_{wv} because of nonconservation of the water vapor mass in the atmosphere. At the considered order of magnitude, D_{wv} is negligible, so the water vapor contribution will not be considered in the expressions of K, BK, CP, and D. However, G_{wv} is a primary process in the budget of enthalpy H_m and it cannot be neglected for the abovementioned reason. The contributions of water vapor in the other primary processes—tendency of H_m, CPV, G_{phase}, G_{diab}, and G_p—have to be kept as well.

e. Budget of eddy kinetic energy

The energetic cycle proposed in L55 was aimed at studying the maintenance of the global circulation, more particularly the transfers between kinetic energy of the zonal mean flow, kinetic energy of the eddy circulations, and available potential energy of the global atmosphere. Consequently, L55 separated the zonal and eddy components of A and K. The eddy components characterize the perturbations with respect to the zonal mean in the global atmosphere. In the L55 analysis, the conversion between zonal kinetic energy K_Z and eddy kinetic energy K_E is referred to as ''barotropic growth'' and the conversion between eddy available potential energy A_E and K_E is referred to as ''baroclinic growth.'' Note that A_E can be produced through a conversion of zonal available potential energy (A_Z) and/or through diabatic processes. The L55 energetic cycle is an attractive concept for studying wave disturbances but, as

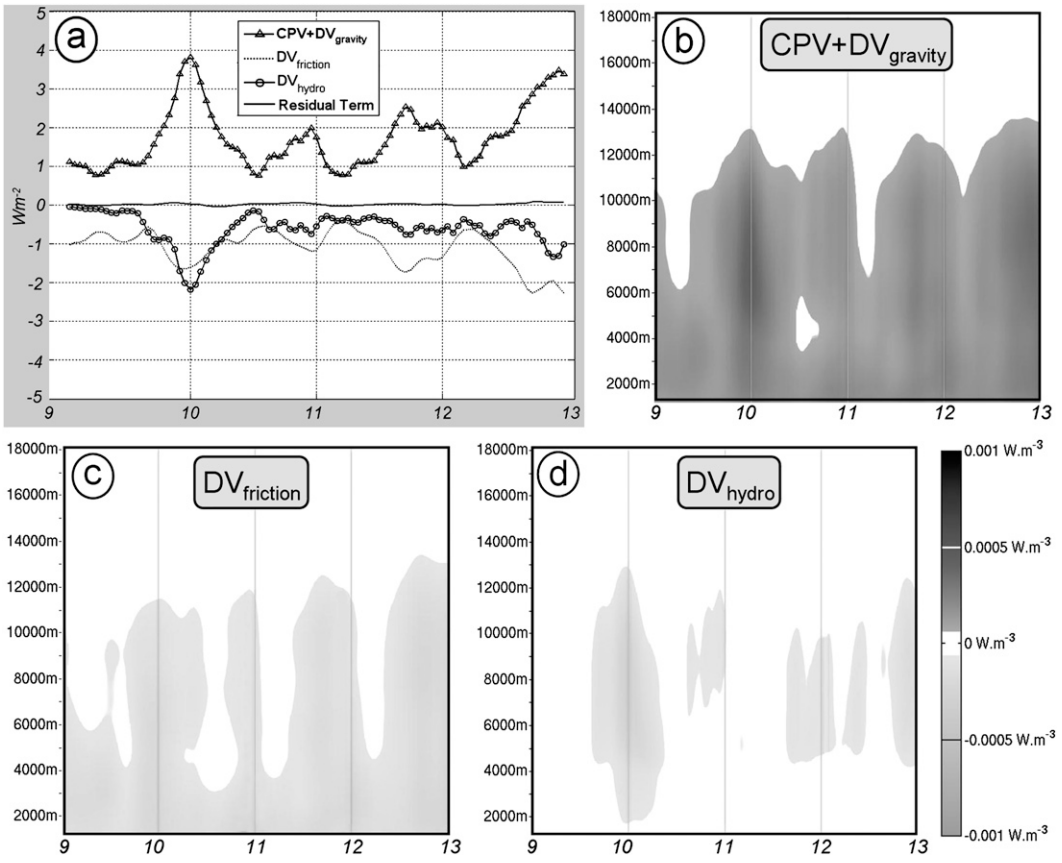

FIG. 11. (a) As in Fig. 5, but for the second-order terms in the budget of KV. The displayed coefficients are the residual term of the first-order terms (solid line with triangles); $DV_{friction}$ (dotted line); DV_{hydro} (solid line with circles); and the second-order residual term (solid line). (b)–(d) As in Fig. 6, but for the second-order terms in the budget of KV.

explained above, it cannot be directly applied to a limited domain.

Applying the theoretical results of section 4, A is replaced by H_m and is not separated in zonal and eddy components, and the energy budget is done in a limited domain. Separating the eddy and zonal components of H_m in the analysis would be meaningful on condition that an unambiguous relation exists between the eddy potential energy and the eddy kinetic energy, which is not straightforward. The conversion between K_E (K_Z) and H_m is referred to as the "eddy (zonal) baroclinic conversion."

Neglecting the water vapor contribution in the horizontal kinetic energy budget, we define the kinetic energies K_Z and K_E as

$$K_Z = \int_{Z_1}^{Z_2} \rho_{a\mathrm{ref}} \frac{\overline{[u]^2 + [v]^2}}{2}\, dz, \tag{33}$$

$$K_E = \int_{Z_1}^{Z_2} \rho_{a\mathrm{ref}} \frac{\overline{u^{*2} + v^{*2}}}{2}\, dz, \tag{34}$$

where $[\cdot]$ denotes a zonal mean in domain D and * indicates a deviation with respect to the zonal mean. As discussed in section 5d, the water vapor contribution cannot be neglected in the first-order terms of the budget of moist enthalpy, so the expression H_m used for the present energy budget is

$$H_m = \int_{Z_1}^{Z_2} \rho_{a\mathrm{ref}} \overline{c_{pm} T}\, dz. \tag{35}$$

Equations for the evolution of K_Z and K_E can be derived from (29) where the second-order terms and the water vapor contribution in the first-order terms are neglected, using the property that $\rho_{a\mathrm{ref}}$ depends only on the vertical coordinate:

$$\frac{dK_Z}{dt} = \mathrm{BK}_Z + \mathrm{CPZ} - \mathrm{CK} + \mathrm{DZ}, \tag{36}$$

$$\frac{dK_E}{dt} = \mathrm{BK}_E + \mathrm{CPE} + \mathrm{CK} + \mathrm{DE}. \tag{37}$$

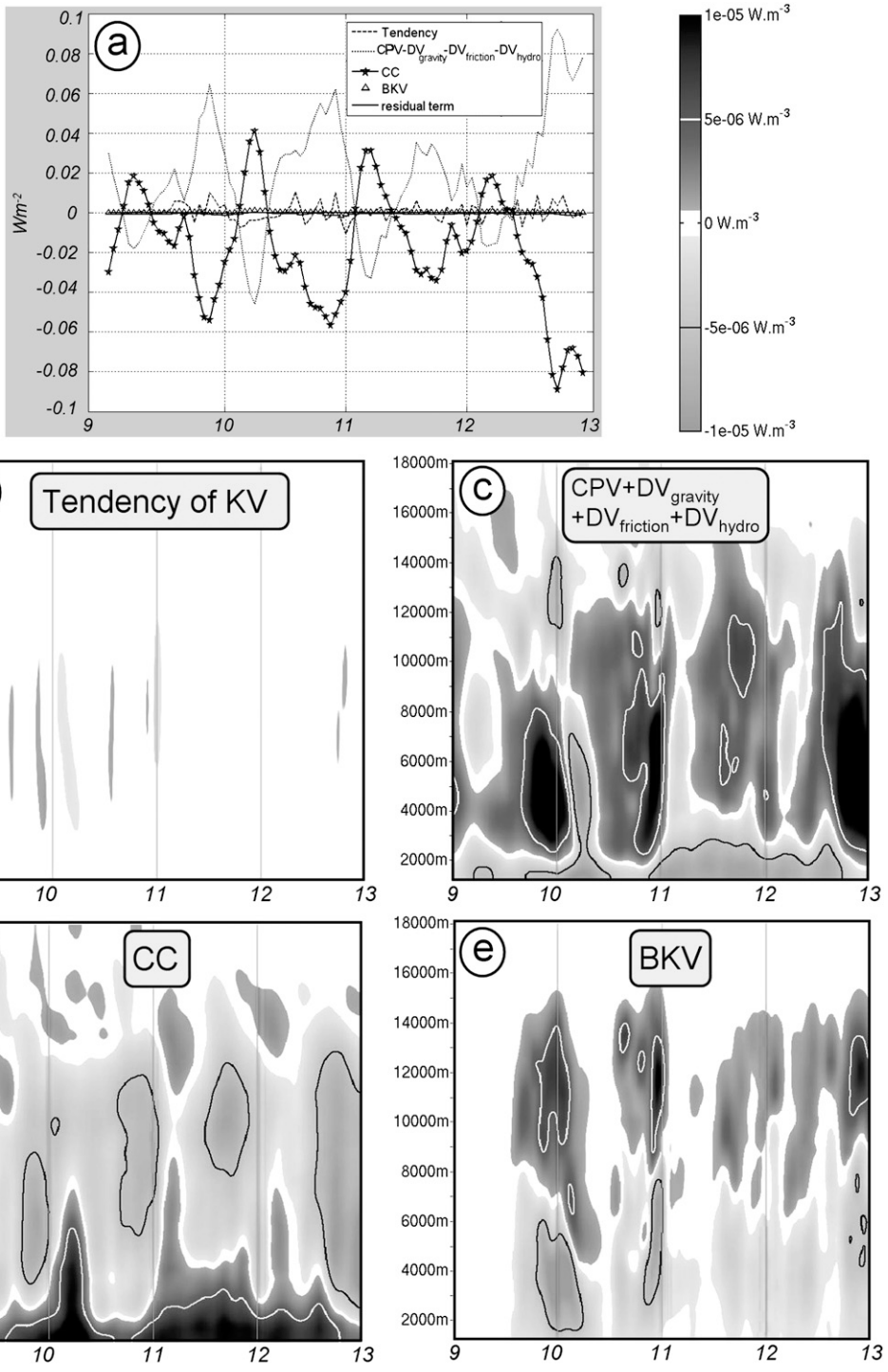

FIG. 12. (a) As in Fig. 5, but for the third-order terms in the budget of KV. The displayed coefficients are the tendency of KV (dashed line); the residual term of the second-order terms (dotted line); CC (solid line with stars); BKV (triangles); and the third-order residual term (solid line). (b)–(e) As in Fig. 6, but for the third-order terms in the budget of KV.

TABLE 1. Classification of the processes involved in the energy budget of section 4d (see Fig. 4) with respect to their magnitude. The middle column indicates the processes' names and the right column gives their order of magnitude in W m^{-3}.

Budget of H_m	Primary processes: BH, CPV, G_{phase}, G_{diab}, tendency, G_p, G_{wv}	$\sim 10^{-1}$ W m^{-3}
	Secondary processes: CP, G_{hydro}	$\sim 10^{-3}$ W m^{-3}
	Tertiary term: G_{residual}	$\sim 10^{-5}$ W m^{-3}
Budget of K	Primary processes: tendency, BK, CP, D_{friction}	$\sim 10^{-3}$ W m^{-3}
	Secondary processes: CC, D_{wv}	$\sim 10^{-5}$ W m^{-3}
	Tertiary term: D_{hydro}	$\sim 10^{-7}$ W m^{-3}
Budget of KV	Primary processes: CPV, DV_{gravity}	$\sim 10^{-1}$ W m^{-3}
	Secondary processes: DV_{friction}, DV_{hydro}	$\sim 10^{-3}$ W m^{-3}
	Tertiary processes: CC, BKV, tendency	$\sim 10^{-5}$ W m^{-3}
	Quaternary term: DV_{wv}	$\sim 10^{-8}$ W m^{-3}

Neglecting G_{residual} and adding terms G_{phase}, G_{diab}, G_{hydro}, G_p, and G_{wv} into G, (32) becomes

$$\frac{dH_m}{dt} = \text{BH} + G - \text{CPV} - \text{CPZ} - \text{CPE}, \quad \text{with} \tag{38}$$

$$\text{BH} = \int_{Z_1}^{Z_2} \overline{\nabla \cdot (\rho_{a\text{ref}} c_{pm} T \mathbf{u})}\, dz, \tag{39}$$

$$\text{BK}_Z = \int_{Z_1}^{Z_2} \overline{\nabla \cdot \left(\rho_{a\text{ref}} \frac{[u]^2 + [v]^2}{2} \mathbf{u} \right)}\, dz, \tag{40}$$

$$\text{BK}_E = \int_{Z_1}^{Z_2} \overline{\nabla \cdot \left(\rho_{a\text{ref}} \frac{u^{*2} + v^{*2}}{2} \mathbf{u} \right)}\, dz, \tag{41}$$

$$G = \int_{Z_1}^{Z_2} \overline{\left[\frac{\rho_{a\text{ref}}}{\rho_a} \frac{\partial p}{\partial t} + \left(\frac{p}{p_{\text{ref}}} \right)^{\kappa} \rho_{a\text{ref}} (\dot{q}_{\text{phase}} + \dot{q}_{\text{diab}}) - \rho_{a\text{ref}} c_{\text{hydro}} \frac{DT}{Dt} + \rho_{a\text{ref}} c_{pv} T \frac{Dr_v}{Dt} \right]} dz, \tag{42}$$

$$\text{CPV} = -\int_{Z_1}^{Z_2} \overline{w \left(\frac{\rho_{a\text{ref}}}{\rho_a} \frac{\partial p}{\partial z} \right)}\, dz, \tag{43}$$

$$\text{CPZ} = -\int_{Z_1}^{Z_2} \left\{ \overline{[u] \left(\frac{\rho_{a\text{ref}}}{\rho_a} \frac{\partial p}{\partial x} \right)} + \overline{[v] \left(\frac{\rho_{a\text{ref}}}{\rho_a} \frac{\partial p}{\partial y} \right)} \right\} dz, \tag{44}$$

$$\text{CPE} = -\int_{Z_1}^{Z_2} \overline{\left\{ u^* \left(\frac{\rho_{a\text{ref}}}{\rho_a} \frac{\partial p}{\partial x} \right)^* + v^* \left(\frac{\rho_{a\text{ref}}}{\rho_a} \frac{\partial p}{\partial y} \right)^* \right\}} dz, \tag{45}$$

$$\begin{aligned} \text{CK} = &\underbrace{-\int_{Z_1}^{Z_2} \overline{[\rho_{a\text{ref}} u^* v^*]} \frac{\partial [u]}{\partial y} dz}_{(1)} \\ &- \int_{Z_1}^{Z_2} \overline{[\rho_{a\text{ref}} u^* w^*]} \frac{\partial [u]}{\partial z} dz - \int_{Z_1}^{Z_2} \overline{[\rho_{a\text{ref}} v^* v^*]} \frac{\partial \overline{v}}{\partial y} dz \\ &- \int_{Z_1}^{Z_2} \overline{[\rho_{a\text{ref}} v^* w^*]} \frac{\partial [v]}{\partial z} dz, \end{aligned} \tag{46}$$

$$\text{DZ} = \int_{Z_1}^{Z_2} \overline{\rho_{a\text{ref}} ([u][F_x] + [v][F_y])}\, dz, \tag{47}$$

$$\text{DE} = \int_{Z_1}^{Z_2} \overline{\rho_{a\text{ref}} (u^* F_x^* + v^* F_y^*)}\, dz. \tag{48}$$

This energetic cycle is schematically displayed in Fig. 13; BH, BK_Z, and BK_E are the boundary terms of the budgets of H_m, K_Z and K_E, respectively, in the limited domain. All the other terms characterize sinks/sources or conversions of energy within this domain. Herein, G is the production/destruction of H_m by diabatic processes; CPV is the vertical baroclinic conversion term between H_m and the vertical kinetic energy KV, and is considered as a sink in the moist enthalpy budget; CPZ and CPE quantify the zonal and eddy horizontal baroclinic production/destruction of K_Z and K_E, respectively; CPE (CPZ) is the work of eddy (zonal) pressure force by the eddy (zonal) circulation; and DZ and DE are the frictional dissipation of K_Z and K_E. When the zonal (eddy) circulation is in geostrophic balance, there is no zonal (eddy) baroclinic conversion. Note that CK corresponds to the barotropic conversion between K_Z and K_E; it is the sum of four terms although it is dominated by the first one: term (1) in (46), related to the eddy meridional transport of eddy zonal momentum. Thus, CK is considered as the conversion between the energy of the zonal mean flow and K_E.

6. Results

a. Eddy vorticity

As seen in Fig. 3, the midlevel trough and ridge of an AEW (characterized by large-scale cyclonic and

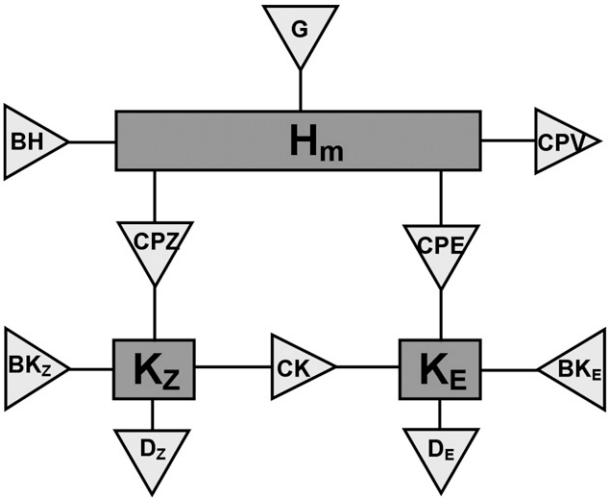

FIG. 13. Schematic view of the energy budget proposed in section 4f. The significance of the energies H_m, KZ, and KE, source/sink terms BH, BKZ, BKE, G, CPV, DZ, and DE, and conversion terms CPZ, CPE, and CK of this budget are explained in the text.

anticyclonic circulations, respectively) are found in domain D, although the pre-Helene disturbance is associated with the midlevel trough only. Hence, it is necessary to objectively determine the respective contributions of the cyclonic and anticyclonic circulations to the eddy perturbation with respect to the zonal mean in domain D.

The eddy vorticity ξ_E, is defined as the vertical vorticity of the eddy horizontal wind,

$$\xi_E = \frac{\partial(v^*)}{\partial x} - \frac{\partial(u^*)}{\partial y}, \tag{49}$$

and is averaged over domain D, so its vertical profile represents the sum of the cyclonic and anticyclonic eddy circulations at each altitude (Fig. 14a). It allows us to determine which of these two circulations predominates in the domain and to evaluate the relevance of the eddy kinetic energy budget to describe the pre-Helene cyclonic circulation. On 9 September, the eddy circulation in domain D was mainly cyclonic below 5000-m altitude and anticyclonic above, which is the signature of the AEW trough associated with the pre-Helene disturbance (see Fig. 3o). On 10 September (Figs. 3p,q), the ridge of this AEW entered domain D to the east and an anticyclonic circulation centered on 28°N, 18°W at 0000 UTC developed in the northwestern part of the considered domain. Hence, the mean value of eddy vorticity became negative down to 1500 m. From 11 September, as the northern anticyclonic circulation moved westward (it was centered on 23°W, 30°N at 0000 UTC and on 27°W, 29°N at 1200 UTC) and the AEW ridge to the east did not intensify, the trough became dominant again. The eddy cyclonic circulation developed vertically up to 10 000 m and its intensity increased gradually near 4000 m. On the afternoon of 12 September, the cyclonic circulation intensified near the surface, which corresponds to cyclogenesis of the simulated Helene.

b. Eddy geostrophic vorticity

The cyclogenetic evolution of an AEW was associated with a pressure decrease, most probably related to the hydrostatic effect of latent heat release associated with deep convection. This can be expressed by the "geostrophic vorticity" ξ_G, which is equal to opposite of the horizontal divergence of the eddy pressure force normalized by the Coriolis parameter:

$$\xi_G = \frac{1}{f}\left\{\frac{\partial}{\partial x}\left[\left(\frac{1}{\rho_a}\frac{\partial p}{\partial x}\right)^*\right] + \frac{\partial}{\partial y}\left[\left(\frac{1}{\rho_a}\frac{\partial p}{\partial y}\right)^*\right]\right\}. \tag{50}$$

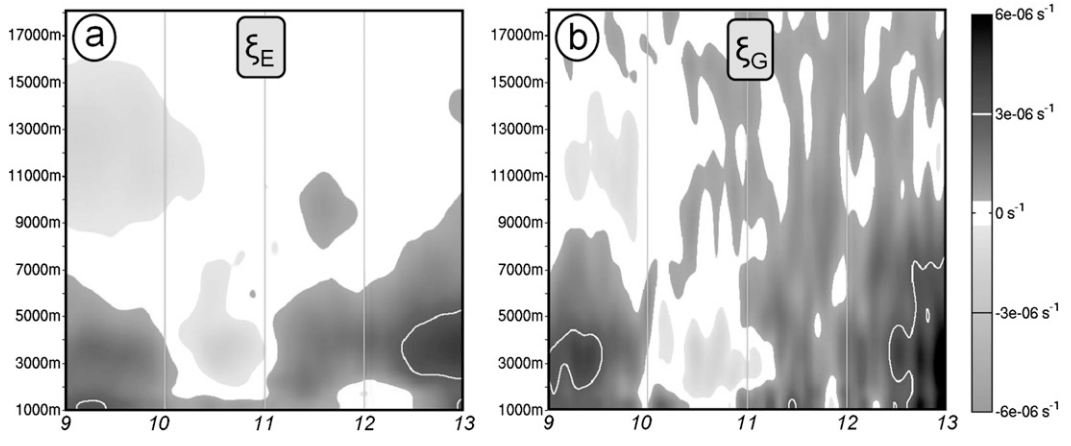

FIG. 14. As in Fig. 6, but for the (a) eddy vorticity ξ_E and (b) eddy geostrophic vorticity ξ_G.

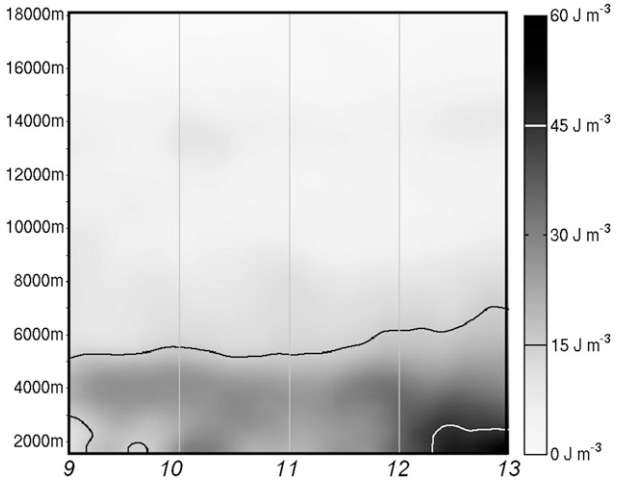

FIG. 15. As in Fig. 6, but for the eddy kinetic energy K_E. The energy (per unit of volume) is in J m^{-3}.

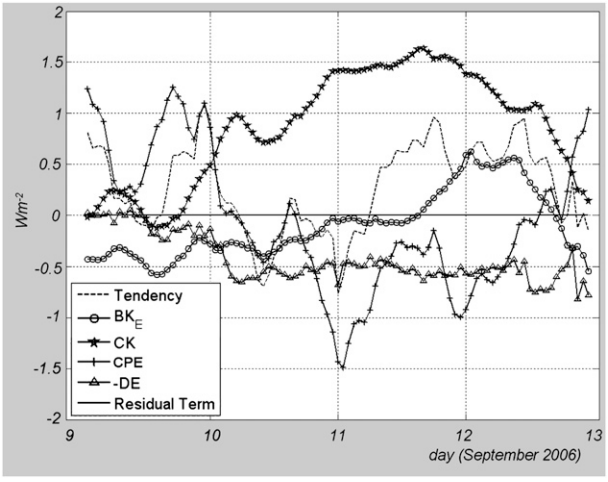

FIG. 16. As in Fig. 5, but for the budget of K_E. The displayed coefficients are the tendency of K_E (dashed line); BK_E (solid line with circles); CK (solid line with stars); CPE (solid line with plus signs); DE (solid line with triangles); and the residual term (solid line).

When this quantity is positive (negative), eddy pressure forces are convergent (divergent) and the pressure perturbation associated with the eddy circulation is negative (positive). Furthermore, ξ_E and ξ_G are equal when the atmospheric flow is geostrophic. The comparison between the mean profiles of ξ_E and ξ_G in Fig. 14 shows that the eddy circulation was approximately geostrophic, which was not certain for such a large perturbation at low latitudes (9°–18°N). On the afternoon of 12 September, however, ξ_E was slightly weaker than ξ_G between 1000 and 8000 m. This suggests that during this cyclogenesis event pressure decreased first, and then geostrophic adjustment of the wind field to the mass field led to an increase of ξ_E.

c. Eddy kinetic energy

The evolution of the vertical profile of K_E (Fig. 15) shows a maximum around 4000 m, which corresponds to the energetic signature of the simulated AEW. On the morning of 9 September, K_E increased between 3000 and 5000 m and then remained approximately constant until the end of the day. On the morning of 10 September a strong increase of K_E in the low levels was followed by a decrease of similar intensity during the afternoon. However, as seen in Fig. 14, at that time the main contribution to the eddy circulation came from the AEW ridge, which played no role in cyclogenesis. From the afternoon of 11 September, K_E increased constantly between 1000 and 5000 m, especially at low levels, in conjunction with the increasing cyclonic vorticity (Fig. 14).

d. Energy budget

Evolution of the vertically integrated terms involved in the budget of K_E is shown in Fig. 16; their vertical profiles are shown in Fig. 17. On 9 September, the first stage of K_E growth was mostly due to eddy baroclinic conversion (CPE > 0), with a positive contribution of barotropic conversion (CK) below 4000 m altitude and a negative one from net advection BKE, except in the lowest levels and between 5000 and 6000 m. This situation is similar to that analyzed by Norquist et al. (1977), who used the inadequate L55 formulation for limited domains but also found that AEW growth over the West African continent is both barotropic and baroclinic. This also meets the idealized case study by Thorncroft (1995) and the space–time spectral analysis by Hsieh and Cook (2007), although these authors did not consider specifically the relationship between energetic conversions and cyclogenetic evolution off shore. Aviles (2004) found smaller baroclinic and barotropic conversions over West Africa for developing cases of AEWs compared to nondeveloping ones. However, the eddy baroclinic conversion in the proposed energy budget does not quantify the same processes as in L55, so it is difficult to compare the present result with previous ones. A new interpretation of this eddy baroclinic conversion term is proposed here.

In particular, it can be noticed that pressure and geostrophic vorticity increased while convective activity was relatively intense during the night of 9–10 September (cf. G_{phase} in Fig. 6d and ξ_G in Fig. 14b). Hence, the eddy circulation was mostly down the eddy pressure gradient in the low to midtroposphere (CPE > 0). This suggests that the wind field was adjusting to the pressure field through horizontal displacement of air. The eddy kinetic energy produced by this horizontal displacement of air through positive eddy pressure work (CPE > 0)

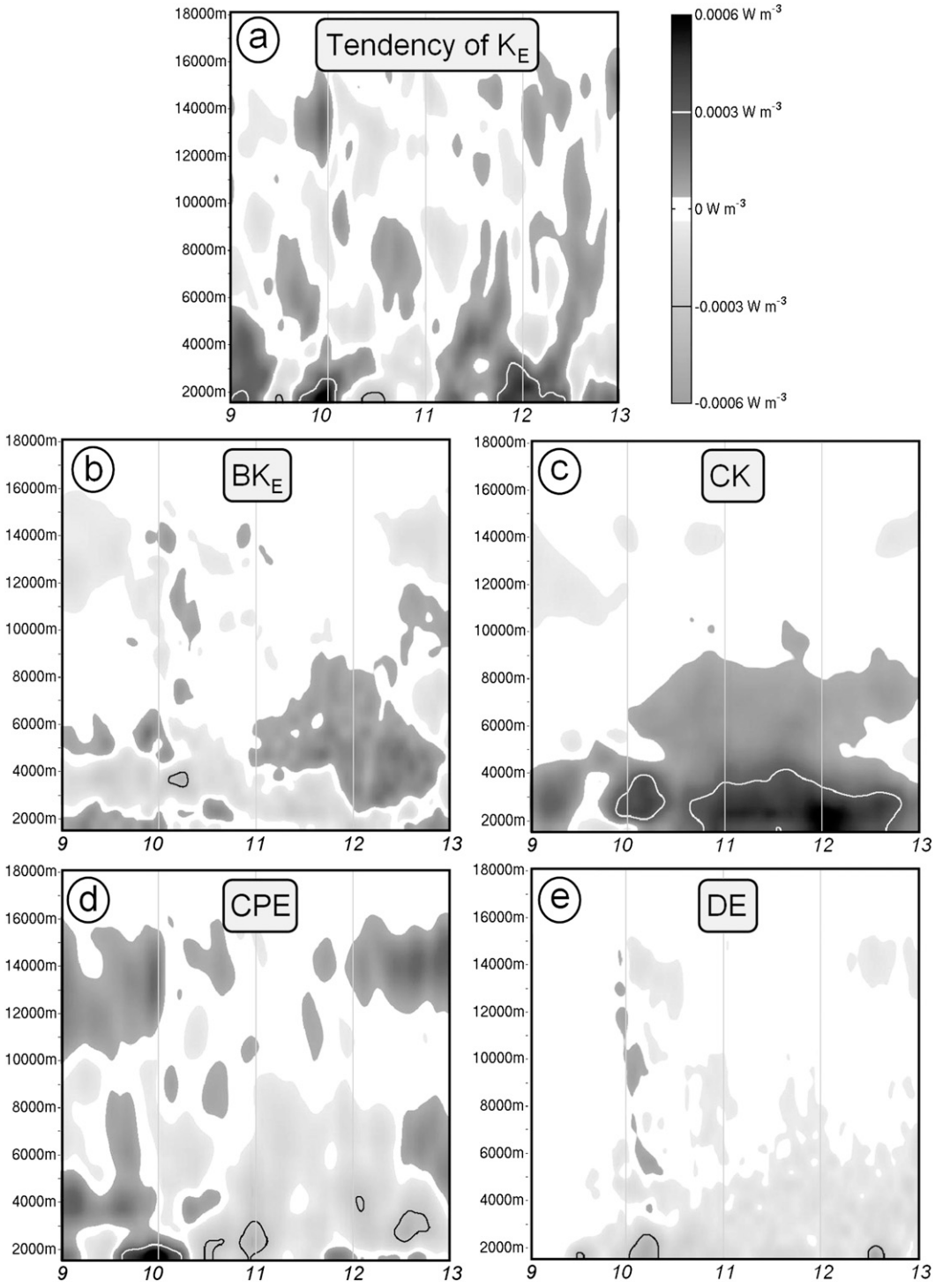

FIG. 17. As in Fig. 6, but for the coefficients in the budget of K_E: (a) tendency of K_E, (b) BK_E, (c) CK, (d) CPE, (e) DE.

was partly exported to the outer flow, as can be deduced from the negative net advection BKE.

The positive barotropic conversion (CK) in the low to midtroposphere from 10 to 12 September was a consequence of the increasingly cyclonic curvature of the easterly flow, in response to the pressure decrease associated with convective activity (Fig. 6d). The negative eddy baroclinic conversion (CPE) indicates that the work

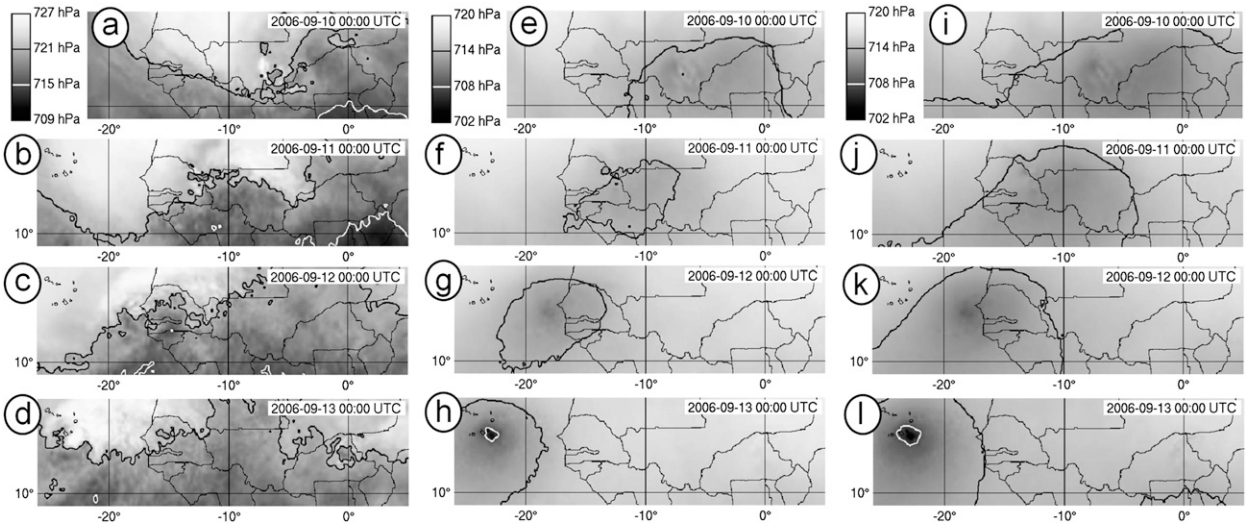

FIG. 18. (a)–(d) $R_a/C_{pa}H_m^A$ (hPa) at 3000 m; (e)–(h) $R_a/C_{pa}H_m^C$ (hPa) at 3000 m; and (i)–(l) total pressure p (hPa) at 3000 m, from (top) 0000 UTC 10 Sep 2006 until (bottom) 0000 UTC 13 Sep 2006. The gray color scale is in the upper left.

of the eddy pressure forces was then negative (i.e., the eddy air circulation was mostly oriented up the eddy pressure gradient). This resulted from the presence of the abovementioned high pressure zone (centered on 29°N, 27°W at 1200 UTC 11 September), which induced a strong northeasterly divergent flow in the western part of domain D (Figs. 3r,s).

The fact that baroclinic conversion became positive again on late 12 September could be the signature of strong convective activity and associated pressure decrease in an environment where the AEJ was weak and the northwestern anticyclonic circulation had moved farther west (at 1200 UTC 12 September, it was centered on 28°N, 32°W). Actually, barotropic conversion decreased on late 12 September because the flow was no longer zonal, but a closed cyclonic and convergent circulation formed instead (Fig. 3u). Thus, some of the kinetic energy created by the positive baroclinic conversion on late 12 September was restored to the outer flow by weak net advection. At that time the system became tropical depression Helene and was able to take enough energy from the sea to be energetically self-sustained (Emanuel 1986).

The observed pressure decrease in this developing system was probably of a convective origin. The next step to investigate this hypothesis would be to more precisely analyze the relation among convection, pressure changes, energy conversions, and the adjustments between mass and wind fields.

7. Perspective for the energetic analysis

To further investigate this problem, we come back to the energetic analysis based on the compressible equations of Bannon (2002). The moist enthalpy in (25) is

$$H_m^C = \rho_a c_{pm} T = \frac{c_{pm}}{R_m} p. \tag{51}$$

Such a relationship cannot be written for the moist enthalpy H_m^A in the anelastic case ($H_m^A = \rho_{aref} c_{pm} T$). In Fig. 18, we show horizontal cross sections at 3000 m of the normalized quantities $R_a/C_{pa}H_m^A$ (Figs. 18a–d) and $R_a/C_{pa}H_m^C$ (Figs. 18e–h) so they can be compared with the total pressure (Figs. 18i–l). Pressure decreased in association with the intensification of pre-Helene disturbance, with minimum values of 711 hPa at 0000 UTC 11 September, 709 hPa at 0000 UTC 12 September, and 702 hPa at 0000 UTC 13 September. This is coherent with the increase of ξ_G observed during this period (Fig. 14b).

The evolution of H_m^C (Figs. 18e–h) is comparable with the evolution of pressure because the moisture correction is small, and the budget of H_m^C can be used to analyze the pressure decrease in the developing AEW. However, the evolution of H_m^A (Figs. 18a–d), which is the adequate thermodynamic variable in Méso-NH, is related to the temperature only, since the density ρ_{aref} is constant at each level. This implies that the processes responsible for the variations of pressure cannot be thoroughly analyzed with the moist enthalpy equation in the anelastic approximation.

Assuming that the processes involved in the budget of H_m^C should have magnitudes comparable to those in the budget of H_m^A, we suggest that in a numerical simulation using compressible equations, the same primary processes would be directly related to the variations of pressure. The residual term of these primary processes would still be linked to the eddy baroclinic conversion.

Consequently, the budget of H_m^C would allow us to quantify the interactions between the vertical circulation forced by convection, pressure decrease, energetic conversions, and adjustment between mass and wind fields.

8. Conclusions and perspectives

The pre-Helene disturbance was associated with an AEW and several MCSs over West Africa during the period before cyclogenesis over the tropical eastern Atlantic near the Cape Verde Islands. A 4-day numerical simulation with Méso-NH using convective parameterization does not exactly reproduce the observed series of these MCSs, but the simulated disturbance shows a relatively similar evolution. The development of this simulated AEW is analyzed with an energy budget adapted from the L55 analysis. Because the energetic analysis of L55 cannot be applied directly in a limited domain, we developed a concept of energy transformations in the atmosphere that can be used locally.

First, considering that there is no robust and versatile definition of available potential energy A for a limited domain, we use the total potential energy E or the enthalpy H to quantify the thermal atmospheric reservoir. We verified that the conversions between E (or H) and K, and between A and K, are equivalent at global scale—the original framework of L55.

Second, we found that in the same hydrostatic framework as L55, the so-called horizontal baroclinic conversion between enthalpy and horizontal kinetic energy can be expressed as the horizontal pressure work resulting from the ageostrophic component of the wind. This means that the horizontal pressure force is a measure of the amount of potential energy that can be converted into horizontal kinetic energy. This result was partly given by Marquet (2003b), although his ''ageostrophic conversion term'' did not appear explicitly in his budget of available potential energy. According to Marquet (2003b), there is a ''potential-energy component which plays the role of vertical distribution of energy by transforming baroclinic into ageostrophic conversions, via unknown processes to be discovered'' (p. 2492). We found that this ageostrophic conversion is actually the horizontal baroclinic conversion between enthalpy and horizontal kinetic energy, so there is no unknown source or sink in this energetic conversion. This definition of horizontal baroclinic conversion is different from that proposed by L55, but it is valid at global and local scales.

Third, we showed that in the most general case (e.g., using compressible equations) the potential energy of the atmosphere can be characterized by the moist enthalpy and that its conversion in total kinetic energy is still proportional to the total pressure work. A positive horizontal (vertical) pressure work corresponds to a growth of horizontal (vertical) kinetic energy. These energy conversions are referred to as horizontal and vertical baroclinic conversions, respectively.

Fourth, the energetic analysis has been adapted to the anelastic equations of Méso-NH. An application to the simulated pre-Helene disturbance confirms that the redefined baroclinic conversions are correctly described with this set of equations. At first order, the tendency of moist enthalpy results mostly from diabatic heating, net advection, and vertical baroclinic conversion. These so-called primary processes show a diurnal cycle similar to that of radiative heating. Convective heating also follows a diurnal cycle with a maximum during the evening. However, convection is also active during the day and the mean vertical velocity in the domain is always positive, although the maximum values occur during the evening. Therefore, the vertical baroclinic conversion is always positive with maximum values during the evening. Variations of pressure due to atmospheric tides and variations of water vapor content have a small but nonnegligible contribution compared to the previous primary processes, so they are considered as primary processes as well. The residual of these primary processes is balanced by the much smaller horizontal baroclinic conversion and total heating rate of hydrometeors. Since the primary processes in the budget of moist enthalpy are partly caused by the vertical circulation of convective origin, convection is associated with pressure decrease, and horizontal baroclinic conversion is related to the adjustment of the wind field to the pressure change, we suggest that there is a physical link between these processes. Other processes theoretically identified in the budget of H_m are negligible.

The tendency of horizontal kinetic energy K results mainly from three primary processes: horizontal baroclinic conversion, net advection, and frictional dissipation. The production/destruction of K is explained by the horizontal baroclinic conversion, with a negative frictional term and weak net advection. Other processes are negligible. In particular, the conversion term between K and the vertical kinetic energy KV, related to the work of the Coriolis force, is a secondary process, so the budget of KV is disregarded and the vertical baroclinic conversion term between H_m and KV is considered as a sink term in the budget of H_m.

Fifth, this simplified energetic analysis is used to derive an energy budget similar to L55. Here, K is separated in the zonal mean K_Z and the eddy contribution K_E. Likewise, the horizontal baroclinic conversion CP is separated in zonal CPZ and eddy CPE components to quantify the baroclinic growths of K_Z and K_E, respectively; CPE (CPZ) is proportional to the work of eddy

(zonal) pressure forces by the eddy (zonal) circulation. When the zonal (eddy) circulation is in geostrophic balance there is no zonal (eddy) baroclinic conversion. The conversion between K_Z and K_E is classically referred to as the barotropic conversion. Unlike in the analysis in L55, however, the enthalpy H_m is not separated into zonal and eddy components, so the energy budget proposed here involves only three energies: H_m, K_Z, and K_E. This energy budget also includes boundary terms, diabatic production of H_m, dissipation of H_m by vertical baroclinic conversion, and frictional dissipations of K_Z and K_E. It is therefore adapted to quantify the respective contribution of large-scale and internal processes to the evolution of eddy kinetic energy of a disturbance such as an AEW in a limited domain.

Our main finding with the energy budget of K_E is that the intensification of the simulated pre-Helene disturbance during its continental stage resulted from both barotropic and baroclinic processes at low and mid levels. This positive baroclinic conversion was associated with a horizontal displacement of air down the eddy pressure gradient in response to a pressure decrease in the trough. The resulting positive eddy pressure work was partly balanced by a negative net advection of eddy kinetic energy. From the afternoon of 11 September over the near-tropical Atlantic, the intensification of the simulated pre-Helene disturbance was associated with a positive barotropic conversion between 1000 and 5000 m and a negative eddy baroclinic conversion between 2000 and 5000 m. The positive barotropic conversion resulted from the decreasing intensity of the AEW entering the considered domain through its eastern limit and the intensifying large-scale motion in the trough region. The negative baroclinic conversion was associated with a horizontal displacement of air up the eddy pressure gradient forced by an external process (i.e., the anticyclonic circulation to the northwest). Finally, on late 12 September, the midlevel tropospheric flow was no longer zonal so barotropic conversion weakened, positive baroclinic conversion started, and some eddy kinetic energy was restored to the outer flow. By then the observed developing AEW was already a tropical depression and was able to take enough energy from the sea to be energetically self-sustained (Emanuel 1986).

Sixth, we showed that the eddy circulation of the simulated pre-Helene disturbance was approximately geostrophic. We propose that the energetic conversions responsible for the observed development might have resulted from an adjustment of the wind field to the pressure decrease induced by convection. In the tropics, because the Coriolis force is not strong enough to lead to a rapid evolution to geostrophic equilibrium, the eddy circulation is therefore convergent and tends to fill up the depression. This is what probably occurred during the continental stage of simulated pre-Helene disturbance. Over the ocean, however, the pressure decrease induced by convection was accompanied by a positive barotropic conversion as the cyclonic curvature of the easterly flow intensified in the low pressure system. The eddy circulation was globally divergent with regard to the westward propagation of an anticyclonic circulation, centered northwest of the trough. In consequence, the wind field adjusted geostrophically to the pressure perturbation induced by convection, a relatively rare event in the tropics. This geostrophic adjustment of the wind following a pressure decrease of convective origin could be the main process responsible for this simulated cyclogenetic evolution off shore. However, in the anelastic case the budget of moist enthalpy cannot be explicitly related to pressure variations, so the link between energetic conversions and this geostrophic adjustment is not explicit, and this hypothesis cannot be further investigated.

At a smaller scale, Rogers and Fritsch (2001) among others have shown that successive convective developments in a mesoscale vortex can reduce the local Rossby radius, which facilitates geostrophic adjustment of the wind field to the mass field. It would be interesting to analyze the adjustment occurring in the pre-Helene disturbance in terms of interactions between the vertical circulation forced by convection, the pressure decrease, and other processes described by the energetic conversion terms. We suggest that a pressure budget deduced from the moist enthalpy Eq. (25) would allow us to quantify this. A numerical simulation resolving the compressible equations of Bannon (2002) can be used for that purpose. In the anelastic case, however, the link between variations of pressure and convection could be investigated with a diagnostic equation of pressure (an example of such a pressure diagnostic in the anelastic case is provided by Smith and Bannon 2008 for a two-dimensional idealized case).

These results will be compared with energy budgets for other developing and nondeveloping cases of AEWs over West Africa and the near-tropical eastern Atlantic. We will also simulate some stages of the pre-Helene and other West African disturbances with Méso-NH at higher resolution with explicit convection. The analysis of the vorticity production by MCSs and their interaction with the developing AEW, at the convective scale and mesoscale, will certainly complement the results obtained from energy budgets at synoptic scale.

Acknowledgments. The present work is part of the first author's thesis at Université Paul Sabatier Toulouse III, France. Based on a French initiative, AMMA was built by an international scientific group and is currently

funded by a large number of agencies, especially from France, the United Kingdom, the United States, and Africa. It has been the beneficiary of a major financial contribution from the European Community's Sixth Framework Research Programme. Detailed information on scientific coordination and funding is available on the AMMA International web site (see http://www.amma-international.org). Numerical simulations were conducted on the CNRS/IDRIS computer under Grants 070591 and 080591. We thank Didier Gazen and Juan Escobar for the technical support in Méso-NH, Dr. Jean-Pierre Chaboureau for the scientific support in Méso-NH, and Dr. Jean-Pierre Pinty for valuable discussions on cloud physics.

APPENDIX

Mathematical Operators

M	Any variable
$\langle M \rangle$	Horizontal integration of M over the surface of the earth
$\tilde{M} = M - \langle M \rangle$	Perturbation of M with respect to its horizontal mean $\langle M \rangle$ over the surface of the earth
$\overline{M} = \overline{M}(z) = \frac{1}{(X_2 - X_1)(Y_2 - Y_1)} \int_{X_1}^{X_2} \int_{Y_1}^{Y_2} M(x, y, z, t)\, dx\, dy$	Horizontal mean of M over domain D delimited by the Cartesian coordinates X_1, X_2, Y_1, Y_2.
$M' = M'(x, y, z) = M - \overline{M}$	Perturbation of M in the domain D with respect to the horizontal mean $\overline{M}$
$[M] = [M](y, z) = \frac{1}{(X_2 - X_1)} \int_{X_1}^{X_2} M(x, y, z, t)\, dx$	Zonal mean of M over the domain (X_1, X_2)
$M^* = M^*(x, y, z) = M - [M]$	Perturbation of M with respect to the zonal mean $[M]$
$\frac{DM}{Dt} = \frac{\partial M}{\partial t} + u\frac{\partial M}{\partial x} + v\frac{\partial M}{\partial y} + w\frac{\partial M}{\partial z}$	Material derivative following the dry air parcel
$\nabla \cdot (M\mathbf{u}) = \frac{\partial (Mu)}{\partial x} + \frac{\partial (Mv)}{\partial y} + \frac{\partial (Mw)}{\partial z}$	Divergence of the quantity $M\mathbf{u}$ using the altitude coordinate

List of Symbols

Superscripts C and A refer to the compressible and anelastic cases. Subscripts v, Z, E refer to the vertical component, zonal mean, and eddy component, respectively. Vectors are in bold.

A	Available potential energy defined by L55
BH	Boundary term (net advection) in the budget of enthalpy
BK	Boundary term (net advection) in the budget of horizontal kinetic energy
BKV	Boundary term (net advection) in the budget of vertical kinetic energy
BK_Z, BK_E	Boundary terms in the budgets of zonal and eddy kinetic energy
C	Horizontal baroclinic conversion term in L55
C'	Supplementary term which appears when the L55 formulation is applied to a finite domain
CC	Conversion term between horizontal and vertical kinetic energies resulting from the work of Coriolis force
c_l, c_i, $c_{\text{hydro}} = r_l c_l + r_i c_i$	Specific heat of liquid water, ice water, and all hydrometeors
CK	Barotropic production/destruction of eddy kinetic energy
CP	Horizontal baroclinic conversion (work of the horizontal pressure force)

c_{pa}, c_{pv}, $c_{pm} = c_{pa} + r_v c_{pv}$	Specific heat of dry air, water vapor, and moist air at constant pressure
CPZ, CPE	Baroclinic production/destruction of zonal and eddy kinetic energy
c_{va}, c_{cv}, $c_{vm} = c_{va} + r_v c_{vv}$	Specific heat of dry air, water vapor, and moist air at constant volume
CVP	Vertical baroclinic conversion
D_{friction}	Frictional dissipation of horizontal kinetic energy
D_{hydro}	Dissipation/generation of horizontal kinetic energy by the work of the momentum forcing of moist air associated with the hydrometeors
$\text{DV}_{\text{friction}}$	Frictional dissipation of vertical kinetic energy
$\text{DV}_{\text{gravity}}$	Dissipation/generation of vertical kinetic energy by the work of gravitational forces
DV_{hydro}	Dissipation/generation of vertical kinetic energy by the work of the momentum forcing of moist air associated with the hydrometeors
DV_{WV}	Dissipation/generation of vertical kinetic energy by condensation/evaporation or deposition/sublimation of water vapor
D_{WV}	Dissipation/generation of horizontal kinetic energy by condensation/evaporation or deposition/sublimation of water vapor
DZ, DE	Frictional dissipation of zonal and eddy kinetic energy
E	Total potential energy defined in L55
f	Coriolis parameter
$(F_x\ F_y\ F_z)$	Cartesian components of the frictional force
g	Acceleration of gravity
G	Total diabatic production/destruction of enthalpy
G_{diab}	Generation/dissipation of moist enthalpy by diabatic processes
G_{hydro}	Generation/dissipation of moist enthalpy by heating of hydrometeors
G_p	Generation/dissipation of moist enthalpy by variations of pressure
G_{phase}	Generation/dissipation of moist enthalpy by latent heat release
G_{wv}	Dissipation/generation of moist enthalpy by condensation/evaporation or deposition/sublimation of water vapor
H_m	Moist enthalpy
K	Kinetic energy
p_{00}	Reference pressure = 1000 hPa
$p = p_a + p_v$	Total pressure
$\dot{q}$	Total diabatic heating rate
$\dot{q}_{\text{phase}}$, $\dot{q}_{\text{diab}}$	Heating rates per unit mass of dry air due to: phase changes and other diabatic processes such as radiation and turbulent dissipation
$\dot{q}_l$, $\dot{q}_i$	Total heating rate of liquid and solid hydrometeors per unit mass of dry air
R_a, R_v	Ideal gas constant for dry air and water vapor
$R_m = R_a + r_v R_v$	Ideal gas "constant" for moist air (this is not a constant)
r_l, r_i, r_{hydro}	Mixing ratio of liquid water, ice water, all hydrometeors
r_v	Mixing ratio of water vapor
t	Time
T	Temperature
$\mathbf{u} = (u\ v\ w)$	Dry air velocity projected in the Cartesian space
$(\dot{u}\ \dot{v}\ \dot{w})$	Cartesian components of the momentum forcing of moist air associated with hydrometeors defined by Bannon (2002)
$(x\ y\ z)$	Coordinates of the Cartesian space
κ	Ratio of ideal gas constant and specific heat at constant pressure (R/C_P) for dry air
$\theta = \dfrac{T}{\pi}$	Potential temperature
ξ_E	Vertical vorticity of the eddy circulation
ξ_G	Geostrophic vertical vorticity of the eddy circulation
$\pi = \left(\dfrac{p}{p_{00}}\right)^K$	Exner function

π_{ref}	Exner function of the reference state in the anelastic case
ρ_a, $\rho_m = \rho_a(1 + r_v)$	Dry and moist air density
$\rho_{a\text{ref}}$	Dry air density of the reference state in the anelastic case
$\langle\sigma\rangle = g\left(\frac{\langle T\rangle}{c_{pa}} - \frac{p}{R_a}\frac{d\langle T\rangle}{dp}\right)$	Static stability of dry air integrated over the surface of the earth
φ	Geopotential
ϕ	Latitude
ω	Vertical velocity in pressure coordinates
Ω	Earth's rate of rotation

REFERENCES

Avila, L. A., and G. B. Clark, 1989: Atlantic tropical systems of 1988. *Mon. Wea. Rev.,* **117,** 2260–2265.

Aviles, L. B., 2004: African easterly waves: Evolution and relationship to Atlantic tropical cyclones. Ph.D. thesis, Dept. of Atmospheric Sciences, University of Illinois at Urbana–Champaign, 212 pp.

Bannon, P. R., 2002: Theoretical foundations for models of moist convection. *J. Atmos. Sci.,* **59,** 1967–1982.

Bechtold, P., E. Bazile, F. Guichard, P. Mascart, and E. Richard, 2001: A mass-flux convection scheme for regional and global models. *Quart. J. Roy. Meteor. Soc.,* **127,** 869–886.

Berry, G. J., and C. Thorncroft, 2005: Case study of an intense African easterly wave. *Mon. Wea. Rev.,* **133,** 752–766.

Bougeault, P., and P. Lacarrère, 1989: Parameterization of orography-induced turbulence in a mesobeta-scale model. *Mon. Wea. Rev.,* **117,** 1872–1890.

Burpee, R. W., 1972: The origin and structure of easterly waves in the lower troposphere of North Africa. *J. Atmos. Sci.,* **29,** 77–90.

Chaboureau, J.-P., and P. Bechtold, 2005: Statistical representation of clouds in a regional model and the impact on the diurnal cycle of convection during Tropical Convection, Cirrus and Nitrogen Oxides (TROCCINOX). *J. Geophys. Res.,* **110,** D17103, doi:10.1029/2004JD005645.

——, J.-P. Cammas, P. Mascart, J.-P. Pinty, C. Claud, R. Roca, and J.-J. Morcrette, 2000: Evaluation of a cloud system life-cycle simulated by Meso-NH during FASTEX using METEOSAT radiances and TOVS-3I cloud retrievals. *Quart. J. Roy. Meteor. Soc.,* **126,** 1735–1750.

——, ——, ——, ——, and J.-P. Lafore, 2002: Mesoscale model cloud scheme assessment using satellite observations. *J. Geophys. Res.,* **107,** 4301, doi:10.1029/2001JD000714.

Dai, A., and J. Wang, 1999: Diurnal and semidiurnal tides in global surface pressure fields. *J. Atmos. Sci.,* **56,** 3874–3891.

Durran, D. R., 1989: Improving the anelastic approximation. *J. Atmos. Sci.,* **46,** 1453–1461.

Emanuel, K. A., 1986: An air–sea interaction theory for tropical cyclones. Part I: Steady-state maintenance. *J. Atmos. Sci.,* **43,** 585–605.

Erickson, C. O., 1963: An incipient hurricane near the West African coast. *Mon. Wea. Rev.,* **91,** 61–68.

Gal-Chen, T., and R. C. J. Sommerville, 1975: On the use of a coordinate transformation for the solution of the Navier–Stokes equations. *J. Comput. Phys.,* **17,** 209–228.

Gray, W. M., 1968: Global view of the origin of tropical disturbances and storms. *Mon. Wea. Rev.,* **96,** 669–700.

Gregory, D., J.-J. Morcrette, C. Jakob, A. M. Beljaars, and T. Stockdale, 2000: Revision of convection, radiation and cloud schemes in the ECMWF Integrated Forecasting System. *Quart. J. Roy. Meteor. Soc.,* **126,** 1685–1710.

Hoskins, B. J., I. Draghici, and H. C. Davies, 1978: A new look at the ω-equation. *Quart. J. Roy. Meteor. Soc.,* **104,** 31–38.

Hsieh, J.-S., and K. H. Cook, 2007: A study of the energetics of African easterly waves using a regional climate model. *J. Atmos. Sci.,* **64,** 421–440.

Kain, J. S., and J. M. Fritsch, 1993: Convective parameterization for mesoscale models: The Kain–Fritsch scheme. *The Representation of Cumulus Convection in Numerical Models, Meteor. Monogr.,* No. 46, Amer. Meteor. Soc., 165–170.

Kiladis, G. N., C. D. Thorncroft, and N. M. J. Hall, 2006: Three-dimensional structure and dynamics of African easterly waves. Part I: Observations. *J. Atmos. Sci.,* **63,** 2212–2230.

Lafore, J. P., and Coauthors, 1998: The Méso-NH Atmospheric Simulation System. Part I: Adiabatic formulation and control simulations. *Ann. Geophys.,* **16,** 90–109.

Laing, A. G., R. Carbone, V. Levizzani, and J. Tuttle, 2008: The propagation and diurnal cycles of deep convection in northern tropical Africa. *Quart. J. Roy. Meteor. Soc.,* **134,** 93–109.

Landsea, C. W., and W. M. Gray, 1992: The strong association between western Sahelian monsoon rainfall and intense Atlantic hurricanes. *J. Climate,* **5,** 435–453.

Lorenz, E. N., 1955: Available potential energy and the maintenance of the general circulation. *Tellus,* **7,** 157–167.

Marquet, P., 1993: Exergy in meteorology: Definition and properties of moist available enthalpy. *Quart. J. Roy. Meteor. Soc.,* **119,** 567–590.

——, 1995: On the concept of pseudo-energy of T. G. Shepherd. *Quart. J. Roy. Meteor. Soc.,* **121,** 455–459.

——, 2003a: The available-enthalpy cycle. I: Introduction and basic equations. *Quart. J. Roy. Meteor. Soc.,* **129,** 2445–2466.

——, 2003b: The available-enthalpy cycle. II: Applications to idealized baroclinic waves. *Quart. J. Roy. Meteor. Soc.,* **129,** 2467–2494.

Norquist, D. C., E. E. Recker, and R. J. Reed, 1977: The energetics of African wave disturbances as observed during phase III of GATE. *Mon. Wea. Rev.,* **105,** 334–342.

Paradis, D., J.-P. Lafore, and J.-L. Redelsberger, 1995: African easterly waves and convection. Part I: Linear simulations. *J. Atmos. Sci.,* **52,** 1657–1679.

Payne, S. W., and M. M. McGarry, 1977: The relationship of satellite inferred convective activity to easterly waves over West Africa and the adjacent ocean during phase III of GATE. *Mon. Wea. Rev.,* **105,** 413–420.

Pinty, J. P., and P. Jabouille, 1998: A mixed-phase cloud parameterization for use in mesoscale non-hydrostatic model: Simulations of a squall line and of orographic precipitations. Preprints, *Conf. on Cloud Physics,* Everett, WA, Amer. Meteor. Soc., 217–220.

Rogers, R. F., and J. M. Fritsch, 2001: Surface cyclogenesis from convectively driven amplification of midlevel mesoscale convective vortices. *Mon. Wea. Rev.,* **129,** 605–637.

Saunders, R., M. Matricardi, P. Brunel, S. English, P. Bauer, U. O'Keeffe, P. Francis, and P. Rayer, 2005: RTTOV-8 Science and validation report. Met Office Tech Rep. NWPSAF-MO-TV-007, 46 pp.

Shepherd, T. G., 1993: A unified theory of available potential energy. *Atmos.–Ocean,* **31,** 1–26.

Smith, J. W., and P. R. Bannon, 2008: A comparison of compressible and anelastic models of deep dry convection. *Mon. Wea. Rev.,* **136,** 4555–4571.

Thompson, R. M., S. W. Payne, E. E. Recker, and R. J. Reed, 1979: Structure and properties of the synoptic-scale wave disturbances in the intertropical convergence zone of the eastern Atlantic. *J. Atmos. Sci.,* **36,** 53–72.

Thorncroft, C. D., 1995: An idealized study of African easterly waves. III: More realistic basic states. *Quart. J. Roy. Meteor. Soc.,* **121,** 1589–1614.

——, and K. Hodges, 2001: African easterly wave variability and its relationship to Atlantic tropical cyclone activity. *J. Climate,* **14,** 1166–1179.